Active Rocket Controls (ARC)

Initial Design Report

Henry Benedictus (Team Lead)

Chyler Bitsoi (CAD lead)

Emilio Huggins (Manufacturing Lead)

AislinnJoy Gacayan (Budget/Fundraising Lead)

Eric Reyes (Communications Lead)

Fall 2025 - Spring 2026

Project Sponsor:

Northern Arizona Rocket Club

Bryan Spouse

Faculty Advisor:

Carson Marty Pete

Instructor:

David Willy

DISCLAIMER

This report was prepared by students as part of a university course requirement. While considerable effort has been put into the project, it is not the work of licensed engineers and has not undergone the extensive verification that is common in the profession. The information, data, conclusions, and content of this report should not be relied on or utilized without thorough, independent testing and verification. University faculty members may have been associated with this project as advisors, sponsors, or course instructors, but as such they are not responsible for the accuracy of results or conclusions.

EXECUTIVE SUMMARY - Emilio Huggins

The Active Rocket Controls (ARC) project aims to design, construct, and test a high-powered level one rocket with an integrated active control system capable of dynamically managing roll about the rocket's longitudinal z-axis. Sponsored by Professor Carson Pete, Northern Arizona Rocket Club and advised by Bryan Sprouse (Yuma Proving Grounds, Hydra-70 Program), this multidisciplinary effort integrates mechanical design, fluid dynamics, and control theory to advance stabilization technologies in amateur rocketry.

The objective is to develop a modular control system that enables both roll induction and roll damping, meeting Tripoli Rocket Association safety and competition standards. The rocket must maintain a controllable ±100 RPM roll for two seconds and stabilize to near zero roll rate, all while maintaining structural integrity under launch loads exceeding 70 lbf. The system must integrate with an Arduino-based flight computer and IMU sensor, maintain a closed-loop latency under 50 ms, and correlate at least 90% between simulation and physical flight results.

To establish a technical foundation, the team benchmarked three primary active control methods; aerodynamic control surfaces (e.g., AIM-9X Sidewinder), thrust vectoring control (e.g., SpaceX Falcon 9), and mass-momentum shifting (e.g., Blue Origin New Shepard). After evaluating each using a weighted decision matrix across six design criteria (cost, mass, reliability, stability, control performance, and manufacturability), the team selected a compressed CO2 thrust vector approach. RockSim simulations and early MATLAB modeling validated the concept against known launch profiles, confirming a feasible trajectory and controllable roll performance.

Preliminary engineering analyses include heat transfer studies of the avionics bay, structural stress verification of 3D printed PLA body sections, and aerodynamic torque calculations. These analyses guide current subsystem prototyping in SolidWorks and Arduino hardware integration. The project's material and component costs remain under the $2000 engineering requirement limit, with the additional funds being raised through GoFundMe and other student-led sales campaigns.

The ARC team's success will be measured through prototype testing and full-scale launches scheduled for January 2026 (system demonstration) and March 2026 (Tripoli-certified flight). By combining modern control theory with additive manufacturing and open-source electronics, this project demonstrates an accessible pathway to actively controlled rocketry, bridging the gap between educational experimentation and emerging aerospace design practices.

TABLE OF CONTENTS

1 BACKGROUND - Aislinn Joy Gacayan

This chapter provides an overview of the Active Rocket Controls Project. It summarizes the project description and the key objectives requested by the client and advisor., including its relevance to the growing aerospace industry. Additionally, it specifies all the major deliverables and what is expected throughout the project. Finally, it describes how success of the project will be measured and what specific standards are to be met.

1.1 Project Description

As the air and space industry evolves to include offensive, defensive, and exploratory missions, active rocket control is essential for precise maneuvering and stability in advancing aerospace technologies. This project focuses on the research, design, and development of systems that are capable of dynamically adjusting a rocket's orientation and stability. The client has asked that multiple methods of control strategy be explored that will then be compared in order to find the most feasible method to assist a high powered rocket. The objective is to stabilize the rocket and induce a roll about the z-axis. The team is provided with an initial budget of $500, but due to additional expenses and requirements, a minimum of $1000 dollars will be fundraised.

1.2 Deliverables

The major deliverables for this project include a model rocket that aligns with level 1 high powered rocket requirements, with an active control system that produces data for analysis and improvement. Additionally, prototyping and simulations are expected throughout the project. The client has requested that test launches are expected in order to test all control mechanisms and electronic components, and has asked for a full literature review. Furthermore, the course requirements include professional and technical assignments such as design reports, presentations, self-learning projects, website and budget plan development.

1.3 Success Metrics

The success of this project will be assessed through various metrics. The control system must adjust orientation about the z-axis, maintaining a roll of 0 +/- 20 degrees while inducing a controlled spin of 100 +/- 10 RMP. The rocket must comply with level 1 rocket requirements, loads, and safety requirements. Key calculations will include structural design analysis on the rocket with 50% of added custom parts. Additionally, they will include other components of flight testing that will be simulated thoroughly before launching. The rocket will need to include sensors that can collect and translate flight data in order for post-flight analysis. It must also include methods in order to be recoverable following any test flights.

2 REQUIREMENTS - Chyler Bitsoi

The Active Rocket Capstone team's goal centers on developing an Arduino-based active control system for a high-powered rocket, 2.5-4 inches in diameter, to meet our customers' challenge of controlling roll rate along the z-axis. The primary goal of this project is to integrate a dynamic control system capable of inducing and stabilizing roll, ensuring it meets the Tripoli Rocket Association safety and competition standards for the 2026 spring demonstration. We will explore different dynamic and control systems, including thrust vector control, cold gas thrusters, and gyroscopic systems, through calculations, simulations, and research methods. We will apply Mechanical Engineering principles such as fluid dynamics, control theory, and structural analysis when researching and developing our rocket systems. Additionally, we will conduct experimentation and simulations using software and prototyping via 3D printing. We aim to build a cost-effective and functional system to ensure feasibility and reliability.

For our process goals, our team is committed to creating a collaborative and organized approach for this project to achieve a score equivalent to an A. To keep our project on track, we will divide the workload evenly amongst our team and into phases: researching different methods, simulations, and building prototypes with Arduino and manufactured components. We will ensure that clear communication amongst our team and clients/advisors is established and maintained throughout the project through regular meetings to report progress and any setbacks. Fundraising and donation requests will fund any additional costs for the construction of the rocket and the required amount set by our instructor. We will ensure proper procedures are followed during our construction, testing, and launch phases of this project.

Our quality goals center on delivering a safe, reliable, and competition-ready high-powered rocket integrated and working control system. We will aim to meet all Tripoli standards and guidelines, and verify all data obtained during our research and development phase of our project to demonstrate a functional system. Our team will follow the Engineering Design process throughout each phase of this project, and contribute a specified amount of time weekly. We not only plan to achieve an A in this class, but also to produce a competition-worthy high-powered rocket that showcases our skills as engineers.

2.1 Customer Requirements (CRs)

Dynamic z-axis control - The system must control the rocket about the z-axis which includes mating stability during flight, and trajectory contorl.
Fits System into a 2.5-4 in diameter body - All components must fit inside a minimum of 2.5 inch and maximum of 4in rocket body, that including motor, motor mounts, avionics bay, and sensors.
Demo Launch - The system must demonstrate functionality in two test phases, a basic flight demonstration by January 2026 and a fully integrated active control demonstration during a Tripoli live test by March 2026.
Sensor Feedback - The control system must be integrated using an arduino based control, and the sensor must be able to record flight data.
Function of no roll and induce roll - The dynamic control system must be able to provide two primary rolls; that being an induced roll for a specified amount of time and stabilized no roll.
Comply and follow Tripoli safety standards - The design must adhere to Tripoli Rocketry Association safety regulations and operational standards for high-powered rocketry. Including a preflight sheet and rocksim validation before launch.
Find the most cost effective solution - The team must explore 3 different methods of active control system and perform a cost analysis to meet the maximum $2000 budget.
Include 3D printed components/parts - At least 50% of the constructed control system must be

manufactured via 3D printing methods.
Deliverables - The project must include all final deliverables such as flight test data, design documentation, and system verification reports as outlined in the sponsor agreement.

2.2 Engineering Requirements (ERs)

Weight Constraint - The total rocket system must not exceed 10lb to ensure flight stability and compatibility with flight vehicles.
Constrained Diameter - All systems must fit into a 2.5 in - 4 in rocket tube diameter.
Z-axis roll control error - The roll orientation error must remain below 2° during active control.
Induce Roll Rate - System must induce and damp roll to 100 RPM within 2 s and then stop rotation.
Control latency - Control loop latency must be under 50 ms to ensure reliable control over the rocket control system.
Dynamic loading capacity - The system must handle aerodynamic and inertial loading of at least 70 lbf.
Reliability - The control system must achieve at least 99% operational reliability during test launches.
Cost constraint - Total system cost should not exceed $2,000.
Custom part integration - At least 50% of system components must be custom fabricated or 3D printed.

2.3 House of Quality (HoQ)

Figure 1: System QFD

3 RESEARCH WITHIN YOUR DESIGN SPACE - Eric Reyes

3.1 Benchmarking

System-Level Benchmarking

To establish a foundation for design, the ARC team analyzed three state-of-the-art active control systems that represent different approaches to rocket stabilization and roll control: aerodynamic control surfaces, thrust vector control, and mass-momentum systems.

"AIM-9x Sidewinder" - Aerodynamic Control Surfaces:

The AIM-9X missile employs movable canards and tail fins to actively control pitch, yaw, and roll via servo-actuated aerodynamic surfaces. This system demonstrates extremely fast response time and high precision during high-speed flight, making it the standard reference for fin-based active control. However, the system's complexity, actuator torque requirements, and need for high-speed servos pose challenges for miniaturization to model-rocket scale. The Sidewinder's control authority serves as a benchmark for evaluating canard-actuated control in the ARC design, which aims to induce controlled ±100 RPM roll within two seconds.

"SpaceX Falcon 9" - Thrust Vector Control:

Falcon 9's engine gimbal system dynamically redirects thrust vector angles to stabilize flight attitude and compensate for aerodynamic disturbances. The design provides high control authority with minimal added aerodynamic drag, but requires complex servo-hydraulic actuation and real-time flight control software. For the ARC project, thrust vectoring was modeled using RockSim to evaluate whether a small-scale gas-jet or micro-nozzle could replicate similar z-axis control.

"Blue Origin New Shepard" - Mass-Momentum Shifting:

Blue Origin's New Shepard vehicle employs an inertial control method through internal reaction control systems and mass shifting for stability during vertical ascent and descent. This approach inspired consideration of a small reaction-wheel or moving-mass mechanism to control roll in the ARC design.

These three systems provide a comparative understanding of control authority, energy efficiency, response time, and manufacturability. Based on this evaluation and the team's decision matrix-

Subsystem-Level Benchmarking

Avionics and Control Hardware:

Open-source flight computers and Arduino-compatible IMU sensors were benchmarked against professional-grade systems such as the *Pixhaw 6C* flight controller. The team determined that an Arduino Nano paired with an MPU6050 or ICM-20948 IMU offers sufficient control-loop speed (<50 ms latency) for closed-loop stabilization at significantly lower cost. This configuration also aligns with literature on Arduino-based flight data collection and PID control tuning for small-scale rockets.

Actuation Systems:

For fin actuation, standard micro-servos (MG90S and DS3218) were compared for torque capacity, response speed, and thermal durability. The MG90S provides up to 2.2 kg*cm torque, sufficient for canard deflection under subsonic flow, whereas high-power servos provide additional torque margin but increase mass and energy consumption. A dual-fin configuration was found optimal, producing ~12.8 ft*lbf of roll moment compared to 4.6 ft*lbf for a four-fin system, reducing drag and complexity.

Structural and Thermal Materials:

Structural benchmarking compared PLA, TPU-95A, and nylon composites for their mechanical strength and temperature resistance. PLA, with an elastic modulus of 3.5 GPa and yield strength of 60 MPa, provided sufficient stiffness and dimensional precision for low-cost 3D printing but demonstrated limited heat tolerance. Thermal modeling of the avionics bay under an assumed common scenario supplied heat load predicted a steady-state temperature of roughly 70°C when unvented, and 61°C when vented, validating the need for airflow slots and reflective shielding in future iterations.

Simulation and Testing Tools:

Rocksim 10 was benchmarked as the primary aerodynamic and trajectory simulator, validated against level 2 flight data with <5% deviation in altitude and velocity predictions. MATLAB scripts were also used to model angular acceleration, torque, and pressure dynamics derived from Reynolds Transport Theory. This dual-software approach ensures 90% correlation between analytical predictions and simulated results, satisfying ER 4 and ER 6.

Summary of Benchmarking Insights:

System-level comparisons demonstrated that while aerodynamic canards and mass-momentum systems offer precise control, thrust vectoring provides the most practical balance between manufacturability, reliability, and control performance at this scale. Subsystem benchmarking validated the selection of Arduino-based avionics for cost-effectiveness, PLA and PETG materials for structural feasibility, and RockSim/MATLAB integration for accurate modeling. Together, these findings informed the design of the ARC rocket as a low-cost, high-performance educational platform demonstrating active control in a small-scale high-powered rocket.

3.2 Literature Review

3.2.1 Henry Benedictus

[1] Tripoli Rocketry Association, *"Unified Safety Code,"* 2025. [Online]. [Accessed: Sep. 08, 2025].
The source discusses the safety regulations that will need to be followed within the TRIPOLI Rocket Association. It ranges from general safety rules, launch pad rules, rocket level rules, such as the size of the rocket motor, and basic model rocket definitions. Since the team will be using TRIPOLI launch sites, this document is important to ensure that the project fits the specific requirements and regulations that TRIPOLI has laid out.

[2] Apogee Components, Inc., *"Peak of Flight Newsletter: When the Data Goes Sideways: Why Your Rocket's Descent Position Might Be Wrong,"* 2023. [Online]. [Accessed: Sep. 08, 2025].
The newsletter is published by Apogee Components and discusses methods to record the orientation of the rocket during flight. A problem that a lot of hobbyist experience is that their altimeters record the ascent with great accuracy; however, they do not record descent with any accuracy at all. "An IMU typically includes three accelerometers (measuring motion in the X, Y, and Z directions) and three gyroscopes (measuring rotation around those axes). These sensors track how your rocket moves and rotates during flight." The IMU can be used to help record the orientation of the rocket during flight. Milligan states 4 different problems IMUs experience that result in inaccurate data. They then discuss different solutions to this problem with the specific sensor. This article is really important because it gives insight into how the team can track the rockets' orientation, and it provides helpful solutions to problems that the project might experience.

[3] M. R. Spakovszky, *Thermodynamics and Propulsion,* MIT Unified Engineering Notes, 2025. [Online]. [Accessed: Sep. 08, 2025].
Dr. Spakovszky created this document that discusses the thermodynamics, propulsion, and heat transfer operations for rockets. The document will be used to find and derive formulas within these fields that can be used for the project.

[4] AIAA OC Rocketry, *"Arduino Tutorials,"* 2025. [Online]. [Accessed: Sep. 09, 2025].
This resource discusses the usage of Arduinos within model rocketry. The topics include materials and supplies, data logging, Intro to GPS on Arduinos, three-axis accelerometer, and many other beginner tutorials for Arduinos. This is vital for the project due to team members having little to no experience working with Arduinos.

[5] Apogee Rockets, *"RockSim Information,"* 2025. [Online]. [Accessed: Sep. 10, 2025].
The article discusses how to use Rocksim, which will be used for the project to simulate the design of the rocket. It is essential to know how to use Rocksim to validate the team's design and to ensure that the rocket meets Tripoli requirements.

[6] P. Moschidis and P. S. Bithas, *"Arduino Rocket Flight Computer,"* in *Proc. PACET,* pp. 1–6, Dec. 2022, doi: 10.1109/pacet56979.2022.9976324.
The paper written by Moschidis and Bithas discusses the processes they took to create an Arduino to collect and record data for a model rocket. They use a sensor that measures barometric pressure, and operates between -500m and 9000m. They then explain how they configured the Arduino. Finally, they explained how they modeled the rocket, tested it, and collected the data. Importantly, they discuss their data analysis process they used. This paper can help lead the team on how the data collection and data analysis should be done.

[7] Dejan, *"Arduino and MPU6050 Accelerometer and Gyroscope Tutorial,"* 2019. [Online]. [Accessed: Sep. 10, 2025].
The tutorial discusses the workings of the MPU6050 IMU (Inertial Measurement Unit), which has an integrated 3-axis accelerometer and 3-axis gyroscope. The author then shows how the IMU is connected to the Arduino and basic code that can be entered into the Arduino to operate the IMU. This tutorial can play a vital role in the design process of the rocket.

[8] W. D. Wassgren, *"Compressible Flow – Converging Nozzle Reading,"* Purdue Univ., ME 30800 Notes, [Online]. [Accessed: Sept. 25, 2025].
The source explains choked flow rate and gives the mass flow rate equation for a choked outlet. Using this equation, the equation for the change of pressure over time was found, which was crucial to finding the force and velocity produced by a compressed CO2 cartridge. It gives an example problem that demonstrates the mass flow rate equation of a CO2 cartridge, showing the equation at work..

[9] N. Nykanen, *"Basics of Angular Acceleration and Rotational Moment of Inertia," R+W America Blog,* 2019. [Online]. [Accessed: Oct. 03, 2025].
The article discusses the relationship between Torque, angular acceleration, moment of inertia, and angular velocity. Using the equations that it provides, the calculated forces, and the moment of inertia of the rocket, the angular velocity in RPMs can be found. Adjusting the forces can help find the needed RPM to satisfy the customer requirements.

[10] F. M. White and H. Xue, *Fluid Mechanics,* 9th ed., New York, NY, USA: McGraw-Hill, 2021. [Accessed: Sept. 29, 2025].
To find the forces of a compressed CO2 cartridge, Reynolds Transport Theory (RRT) was used to find the change in Force over time with the change in velocity and pressure of the cartridge. Given the basic RTT found in Chapter 3, velocity was added in the control volume and system to find momentum. When taking the integral of momentum of the control volume and system, the result is the sum of the forces of the cartridge.

3.2.2 Aislinn Joy Gacayan

[11] S. Ainsworth, *"A Guide to Optimal Altitude: Part 2,"* Apogee Rockets Newsletter, 2015. [Online]. [Accessed: Sep. 14, 2025].
This source describes rocketry fundamentals and explains how burn time correlates with altitude. It explores how to maximize the altitude given different factors such as burn time, drag, and loss due to gravity. It also provides graphical visualization of how those factors affect altitude over time. The simulation modeling provides a good example of what will be expected for simulation testing in our project. It is also useful for analysis of different factors that will affect the flight of the rocket.

[12] G. P. Sutton and O. Biblarz, *Rocket Propulsion Elements,* 9th ed., Hoboken, NJ, USA: Wiley, 2017.
This textbook provides a detailed discussion of various rocket propellants, their associated propulsion systems, and fundamental principles. It covers principles of thermodynamics, fluid mechanics, as well as different types of systems and components of rocket propulsion. This source is relevant to the project because part of the requirements includes applying principles of fluid dynamics to the analysis of the rocket's performance.

[13] Tripoli Rocketry Association, Inc., *"NAR-TMT Combined Motor List,"* 2025. [Online]. [Accessed: Sep. 14, 2025].
This source is a catalog listing motors certified by the National Association of Rocketry (NAR), the Canadian Association of Rocketry (CAR), and Tripoli Rocketry Association (TRA), along with their characteristics. It provides each motor type, the dimensions, impulse time, mass, and more. This applies to the project as it gives general motor information to utilize as a standard, as well as for comparison when selecting what motors to use.

[14] AeroTech Consumer Aerospace, *"AeroTech Master Motor Matrix,"* updated Apr. 2, 2023. [Online].
This source is a matrix that lists AeroTech certified motors and their related characteristics. This includes dimensions, casing sizes and propellant, impulse, and weight. This also provides comparable information of different motor types in order to have a standard set of data to reference.

[15] NASA Glenn Research Center, *"Specific Impulse" and "Rocket Thrust Summary,"* 2025. [Online]. [Accessed: Sep. 15, 2025].
This source presents simplified equations relating to impulse and thrust. It provides a brief summary and necessary equations for the specific impulse of a rocket. This source was utilized to aid in the calculation requirement of the project. Specifically, in calculating the total impulse that needed to be produced by the motor. It was then used to help find the change in velocity over time when there was a change of pressure over time of a compressed CO2 cartridge.

[16] S. Bundalevski, V. Cingoski, and S. Gelev, *"Determination of the Total Impulse of the Solid Rocket Motor by Using Two Mathematical Methods,"* in *Proc. IT (SPIT),* 2018, pp. 1–3, doi: 10.1109/SPIT.2018.8350456.
This paper describes methods for calculating the total impulse of solid rocket motors. The methods used include fixing nonlinear regression models to thrust vs time data that is compared to mathematical modeling in order to determine the total impulse. This source is relevant as it aids in the calculations that must be performed as part of the extensive analysis that will be needed for the project.

[17] A. Praveen et al., *"Thrust Vector Control of Solid Propellant Model Rocket,"* in *Proc. INCOFT,* 2023, pp. 1–6, doi: 10.1109/INCOFT60753.2023.10425646.
This source reports on the control of thrust direction in a solid propellant rocket, including experimental results. It describes mechanical actuation and joint design that is used in the thrust vectoring method of control. This is relevant to the project as part of the requirements is to research various methods of control systems that can be compared in order to select the most suitable method for the project.

3.2.3 Chyler Bitsoi

[18] RocketPy Documentation, *"Roll Equations for High-Powered Rockets,"* 2025. [Online].
This source goes over the various force equations on a high powered rocket, particularly in correlation with different fin geometries. This source was particularly helpful to calculate the torque required by server motors to induce a controlled roll on our proposed rocket.

[19] R. Nakka, *"RD_fin — Rocket Fin Design and Aerodynamics,"* 2025. [Online].
This source goes over the various components or a high powered rocket fin, along with various aerodynamic forces acting on a rocket. This source was helpful in identifying major components significant to rocket fin design. Additionally this source was significantly helpful in designing a baseline for our rockets fin, in order to conduct Rocksim simulation to establish a design matrix for our rocket motor.

[20] NASA, *"The Practical Calculation of Aerodynamic Characteristics of Slender Finned Vehicles,"* 1967. (Barrowman Report).
This source goes over the derivation and real world application of John Barrowman equation necessary for finding force and roll moment on high powered rocket fins. Additionally this source could be used as benchmarking and engineering standards to validate my fin calculations.

[21] *"Introduction to Rocket Design,"* 2025. [Online].
This source discusses the basic design of rocket components such as fins and nozzles, including their characteristics and technical details. This source is particularly useful to see the effects of different rocket components on this flight and stability. This source was also important for a baseline design to start our design process and rocket simulations.

[22] *"An Actively Stabilised Model Rocket,"* Research Paper, 2025.
This research paper provides an overview of basic control systems that can and have been used in rockets, including gyroscopes and gimbaled motors for thrust vectoring. Particularly this source was helpful to see the effects of how active rocket rocket fins are controlled via control systems like ardinuo. Additionally this source was used to see the limitations of an active fin control via the control like max deflection.

[23] J. D. Anderson, *Fundamentals of Aerodynamics,* latest ed., New York, NY, USA: McGraw-Hill.
This source reviews the fundamentals of aerodynamics, including different flow regimes and significant equations relevant to fin and rocket design. Additionally this source can be used as engineering standards and reference for various equations used, such as center of pressure and gravity. This textbook will also be helpful when CFD simulations will be conducted to further understand aerodynamic forces on our rocket.

[24] *"Design of a Servo Mechanism for Controlling Missile Fins in Pitch and Yaw Planes,"* Research Paper.
This source discusses servo motor integration and design, including design equations and supporting references. Additionally the servo torque equation was particularly helpful when staring the design of our server motor, and required forces to induce a specified toqure. Additioanlly this source could be used as engineering stanards to validate our calculations for server mechanism.

[25] *"Model Rocket Guidance by Canards,"* Research Paper.
This source explains how actuated canards can be integrated into a rocket to induce roll via a control system. This source explores another method for our active control fin system, via a frontal mount active

canard rather than an aft fin.

3.2.4 Eric Reyes

[26] NASA Glenn Research Center, *"Rocket Center of Gravity," Beginner's Guide to Aeronautics,* 2025. [Online].
This source explains how to calculate the center of gravity (CG) of a rocket by breaking it down into its components and using their masses and positions. It walks through the basic equations in a way that's easy to follow and gives a good foundation for understanding why CG matters for stability. Since it comes directly from NASA Glenn, it's reliable and also written with students in mind, which makes it practical for applying in a project setting.

[27] T. Van Milligan, *Numeric Methods in Model Rocket Design,* Apogee Rockets, Tech. Pub. #17.
Van Milligan's technical guide covers methods for calculating the center of pressure (CP), including the classic Barrowman equations and numerical approaches. It is geared toward model rocketry, but the math and process are directly applicable to larger experimental rockets. What makes this source useful is that it does not just give formulas; it also explains how to apply them step by step when working through a design to make sure the stability margin is acceptable.

[28] T. Van Milligan, *"How to Find the Center of Pressure on a Rocket,"* Advanced Construction Video, 12:50, Apogee Rockets.
This video provides a visual explanation of how to locate the CP on a rocket and why it is important for stability. Van Milligan demonstrates the process in a hands-on way, which helps make the concepts easier to understand than just reading them on paper. It is especially helpful for seeing how CP relates to CG and how to check that the stability margin is in the safe range before flight.

[29] ESRA, *International Rocket Engineering Competition Rules & Requirements,* ver. 1.6, 2025. ~Engineering Standard.
The ESRA rules outline what teams have to include in their technical documentation, including CG, CP, and the calculated stability margin. These are required for a rocket to be considered flight-ready in competition. For that reason, this source acts as both a guideline and a standard, making sure every team measures stability the same way and meets a baseline level of safety before launch.

[30] G. Solomon and Y. Abreham, *"Analytical Calculation on Rocket Stability," Int. J. Res. Anal. Reviews,* vol. 7, no. 3, 2020.
This paper looks at how fin geometry changes affect CG, CP, and overall stability. The authors go through different fin designs and show how they shift aerodynamic stability. It backs up the idea that design tweaks like changing fin size or shape can be predicted analytically before actually building. For a project, this gives extra confidence in using equations to model stability instead of relying only on trial and error.

[31] R. Cadamuro, M. P. Cardillo, and L. F. Macaluso, *"A Static Stability Analysis Method for Passively Stabilized Sounding Rockets," Aerospace,* vol. 11, no. 3, p. 242, 2024.
This article updates stability analysis methods for sounding rockets and focuses on cases where the rocket does not use active control systems. It shows how CG and CP placement directly tie to flight performance and introduces refinements to traditional methods. Since it bridges small-scale model rockets and larger sounding rockets, it is a solid reference for teams working on educational rockets that still need to demonstrate safe passive stability.

[32] J. Barrowman, *"TIR-33: Calculating the Center of Pressure of a Model Rocket,"* Nakka-Rocketry, [Online].
Barrowman's original work lays out the equations for calculating CP on rockets, which are still the standard today. The method breaks the rocket into parts like the body tube, nose cone, and fins, and then calculates how each contributes to CP location. Even though it was written decades ago, it is still one of the most cited references in rocketry design because of how simple and effective the method is. Most modern tools and textbooks build on this approach.

[33] A. Downey, *Vibration Mechanics: A Practical Introduction,* Clemson (SC): SC University Publications. [Online].
Concise, practical treatment of damping, damping ratio (ζ), and how added structural damping shifts system response. For ARC, the concepts guide sensor-bay mounting and avionics isolation: selecting viscoelastic interfaces to raise loss factor, targeting ζ to keep transmissibility below unity near structural resonances, and ensuring IMU readings aren't corrupted by chassis-borne vibration during boost and through motor burnout.

3.2.5 Emilio Huggins

[34] *"Compression Tests of Tubing Used in Rocketry,"* Newsletter.
This source examines compression tests of rocket tubing and body sections to evaluate structural performance and failure modes. It details the use of standardized stress analysis methods to determine yield limits, buckling tendencies, and load-bearing capacity of typical model rocket materials. These findings guide the team's structural verification for 3D-printed and composite components under compressive launch and recovery loads. Understanding how thin-walled rocket tubes fail under axial stress provides a basis for selecting appropriate wall thicknesses and reinforcement patterns for the ARC prototype.

[35] *"Unified Analysis of Aerospace Structures through Implementation of Rapid Tools into a Stress Framework,"* Technical Report.
This report presents the integration of rapid analysis tools within the HyperSizer framework to streamline aerospace structural design. The approach improves traceability, verification accuracy, and compliance with FAA certification standards. For ARC, this methodology informs how to validate the strength and stiffness of printed components using simplified finite-element analysis (FEA) and cross-sectional stress models. It establishes a traceable workflow for iterating between CAD geometry, loading conditions, and safety factors, ensuring the rocket body meets design margins for launch and recovery.

[36] *"3D Printing Temperature: Effects, Materials and Considerations,"* Technical Guide.
This guide reviews how filament type, extrusion temperature, and cooling conditions influence the mechanical properties and dimensional accuracy of 3D-printed parts. It compares common thermoplastics such as PLA, PETG, ABS, and nylon, highlighting their tensile strength, softening points, and thermal deformation limits. These insights are directly applied to the ARC avionics bay and fin-mount designs, where internal heat sources and aerodynamic friction require material choices with sufficient thermal stability and low warpage during flight

[37] *"Structural Design and Analysis of High-Powered Model Rockets Using OpenRocket,"* Journal.
This journal article presents an in-depth structural analysis of model rockets using OpenRocket simulation software. It covers aerodynamic modeling, center-of-gravity (CG) and center-of-pressure (CP) calculations, and material selection for stability optimization. For ARC, this paper provides the framework for coupling OpenRocket's analytical outputs with RockSim validation to predict static

stability margin and ensure proper fin sizing and placement for stable ascent under active roll control conditions.

[38] R. Nakka, *"Nosecone Design,"* Technical Tutorial.
This tutorial discusses how nosecone geometry—such as ogive, conical, and Haack series shapes—affects aerodynamic drag, pressure distribution, and stability. It provides governing equations for drag coefficient estimation and guidance on selecting profiles suited for subsonic and transonic regimes. The ARC team used these insights to select a Haack-series profile with a drag coefficient of approximately 0.15, balancing aerodynamic efficiency with manufacturability through 3D printing.

[39] *"Reaction Wheel Based Rocket Active Spin Stabilization,"* Research Paper.
This paper examines an alternative stabilization strategy that uses a reaction wheel to counteract roll disturbances and maintain attitude. The research outlines the control laws, feedback sensor integration, and experimental flight data for a small-scale rocket. While ARC ultimately selected aerodynamic control surfaces, the reaction-wheel method served as a comparative benchmark for evaluating internal mass-momentum control and energy efficiency trade-offs during the concept selection phase.

[40] *"Introduction to Rocket Design 9. Recovery System,"* Technical Tutorial.
This paper examines an alternative stabilization strategy that uses a reaction wheel to counteract roll disturbances and maintain attitude. The research outlines the control laws, feedback sensor integration, and experimental flight data for a small-scale rocket. While ARC ultimately selected aerodynamic control surfaces, the reaction-wheel method served as a comparative benchmark for evaluating internal mass-momentum control and energy efficiency trade-offs during the concept selection phase.

3.3 Mathematical Modeling

3.3.1 Angular Velocity Produced by Compressed Gas

To find the angular velocity produced by compressed gas exiting from the sides of the rocket, the force of the gas must be found first. First, by using the Reynolds Transport Theory (RTT), which is a "bridge that connects the mathematics between a system of individual masses and a specific region specified as the control volume"[9th ed].

$$\sum F = \frac{d}{dt}\int_{CV} \rho v dV + \int_{CS} \rho c(v \bullet n) dA \qquad (1)$$

$$\rightarrow F = \dot{m}v + (P_0 - P_{atm})A_e \qquad (2) \qquad [10]$$

$$\rightarrow F(t) = (Kv_e(t) + A_e\beta)P_0 e^{-\lambda t} - A_e P_{atm} \qquad (3)$$

The equations above show the derived version of the RTT. Where CV is the control volume, which is the air canister, and CS is the control system, which is the remainder of the system. Velocity was entered into the CV and CS to create a moment equation, in which the integral of momentum is taken to provide a force equation. The integrated equation shown in equation 3, doesn't account for a change in pressure over time, which then needs to be found.

$$-\dot{m}_{Choked} = -\left(1 + \frac{\gamma-1}{2}\right)^{\frac{1+\gamma}{2(1-\gamma)}} * p_e\sqrt{\frac{\gamma}{RT_0}}A = -KP_0 \qquad (4)$$

$$K = \left(1 + \frac{\gamma-1}{2}\right)^{\frac{1+\gamma}{2(1-\gamma)}}\sqrt{\frac{\gamma}{RT_0}}A_e \qquad (5)$$

$$\frac{d}{dt}\left(\frac{P(t)V}{RT_0}\right) = \frac{V}{RT_0}\frac{dP}{dt} = KP_0 \rightarrow \frac{dP}{dt} = -\left(\frac{KRT_0}{V}\right)p_0 \quad (6) \quad [8]$$

$$P(t) = P_0 e^{-\lambda t} \; where \; \lambda = \left(\frac{KRT_0}{V}\right) \quad (7)$$

$$\beta = \left(1 + \frac{\gamma-1}{2}\right)^{\frac{1+\gamma}{2(1-\gamma)}} \quad (8)$$

Equations 9-12 uses the Choked Mass Flow rate equation to find the change in pressure over time. It creates an exponential decay line, which shows the decrease in pressure over time. From equation (3), the exit velocity of the needs to be found. Using the equations below, the final exit velocity is found by plugging in the equation (7) since pressure dictates the velocity of the gas.

$$h_0 = h + \frac{v^2}{2} \quad (9)$$

$$h_0 = C_p T_0 \qquad h = C_p T_e \qquad P_0 = P(t) \qquad C_p = \frac{\lambda R}{\gamma-1}$$

$$C_p T_0 = C_p T_e + \frac{v_e^2}{2} \rightarrow v_e^2 = 2C_p(T_0 - T_e) \quad (10)$$

$$\frac{T_e}{T_0} = \left(\frac{P_e}{P_0}\right)^{\frac{\lambda-1}{\lambda}} \rightarrow T_e = T_0\left(\frac{P_e}{P(t)}\right)^{\frac{\lambda-1}{\lambda}} \quad (11)$$

$$v_e = \sqrt{2\frac{\lambda R}{\lambda-1}T_0\left[1 - \left(\frac{P_e}{P(t)}\right)^{\frac{\lambda-1}{\lambda}}\right]} \quad (12)$$

Equations (7), (8) and (12) can now be integrated into equation (3) to find the change in force over time produced by compressed air. With the force found, the angular velocity of the rocket in RMP can be found using equations ()-(), which shows the relationship between force, moment of inertia, and angular velocity.

$$\alpha = T/I \quad (13)$$

$$I = \frac{1}{2}M(r_2^2 + r_1^2) \quad (14)$$

$$\alpha = \frac{\omega}{t} = \frac{\pi RPM}{30t} \quad (15)$$

$$RPM = \frac{30\alpha}{\pi} \quad (16)$$

To visualize the change in RPM, force, velocity, and pressure over time, MATLAB code was used. The equations above were entered with assumed conditions expressed in the table below. The final subplots are shown within figure 2. The code can be found within Appendix 1.

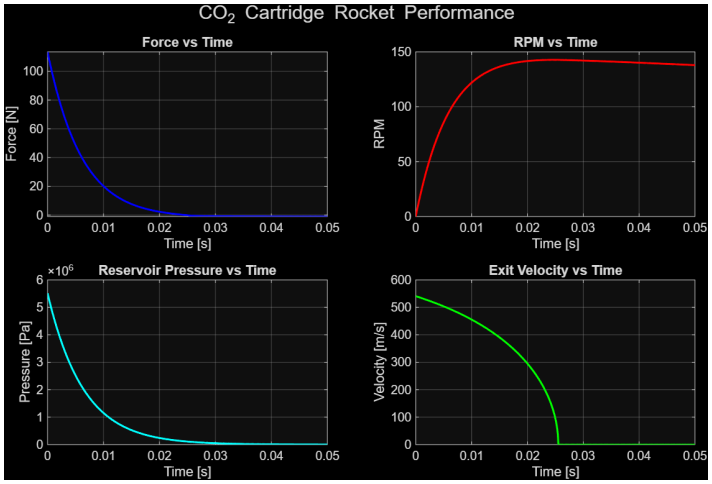

Figure 2: Visualization of Formulas (1), (2), (3), and (4)

$\gamma = Ratio\ of\ Specific\ Heat\ (C_p/C_v)\ (1.289)$

$A_e = Exit\ Area\ (m^2)\ (1 * 10^{-5} m^2)$

$\dot{m} = Mass\ Flow\ Rate\ (kg/s)$

$P_0 = Pressure\ (Pa)(5.5158 * 10^6 Pa)$

$P_a = Ambient\ Pressure\ (Pa)(1.01325 * 10^5 Pa)$

$T_0 = Internal\ Temperature\ (K)(293.15K)$

$R = Specific\ Gas\ Constant)(188.92 \frac{J}{kgK})$

$\rho = Density\ (kg/m^3)\ (1.98 kg/m^3)$

$\dot{m} = Mass\ Flow\ Rate\ (kg/s)$

$H = Power$

$\omega = Angular\ Velocity$

$T = Torque\ (Nm)$

$C_p = Specific\ Heat\ Constant$

$r_2 = Outer\ Radius\ (m) = 0.028829m$

$r_1 = Inner\ Radius\ (m) = 0.02m$

$F = Force\ (N)$

List of Assumptions and Units for Equations for 3.3.1

3.3.2 Thermal Resistance

In order to evaluate the thermal resistance required of the capsule and materials used to house the rocket motor, an analysis was done on the standard model rocket body design. Figure __ shows the general layout of a standard model rocket capsule.

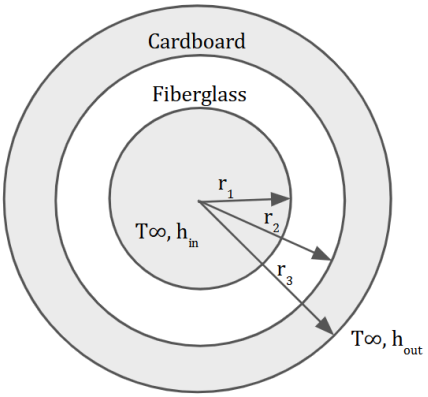

Figure 3: Cross-Sectional Diagram of Model Rocket Materials

The equations required to analyze this included the resistance due conduction and convection, as well as the total resistance. The case of the standard model rocket was broken down into a thermal circuit starting with the motor on the inside.

$$R_{t,cond} = \frac{ln(\frac{r_2}{r_1})}{2\pi kL} \quad (17)$$

$$R_{t,conv} = \frac{1}{h2\pi rL} \quad (18)$$

$$R'_{tot} = \Sigma R_i \quad (19)$$

This resulted in a total resistance for the model of 4.134 K/W. If the materials or design of the motor housing is changed, it still needs to be able to resist any heat produced by the motor during its burn time. The results were also found for individual materials for a general comparison. This resulted in $R_{PLA} < R_{Wood} < R_{Cardboard} < R_{Fiberglass}$.

$$R'_{tot} = 4.134 \frac{K}{W}$$

$$R_{Cardboard} = 1.29 \frac{K}{W} \quad (20)$$

$$R_{Fiberglass} = 2.149 \frac{K}{W} \quad (21)$$

$$R_{PLA} = 0.496 \frac{K}{W} \quad (22)$$

$$R_{Wood} = 0.537 \frac{K}{W} \quad (23)$$

Additional assumptions and units can be seen below

R = Thermal Resistance [K/W]	L = Length [m]
h = Convection Coefficient [W/m2K]	r = radius [m]
k = Thermal Conductivity Coefficient [W/mk]	T = temperature

$k_{Cardboard}$ = 0.05 W/mk	L = 0.203 m	h_{in} = 100 W/m2K
$k_{Fiberglass}$ = 0.03 W/mk	r_1 = 0.035 m	h_{out} = 10 W/m2K
k_{PLA} = 0.13 W/mk	r_2 = 0.038 m	
k_{Wood} = 0.12 W/mk	r_3 = 0.0415 m	

3.3.3 Servo Torque and Fin Moment/Force.

To induce a control roll on a high-powered rocket, a roll moment must be induced using active actuating fins. The following mathematical modeling is the evaluation of the required fin forces to induce a 100 RPM roll about the rocket's z-axis and to dampen the roll in order to stabilize flight. These models guide key design decisions, including fin sizing, number of fins, servo requirement, and overall control strategy.

The governing equation is Newton's second law of rotational motion. Which other equations were further derived, which also includes correlations using Barrowman rocket equations. Where I_z is the axial mass moment of inertia and ω is the angular velocity.

$$I_z\omega = M_{roll} \quad (24)$$

The aerodynamic lift produced by deflected rocket fins is identified as L below. Where q is the dynamic pressure, S is the reference fin area, and Cc is the lift curve slope per radian, and δ is the fin deflection angle.

$$L = qSC_{c\alpha}\delta \quad (25)$$

The total roll moment in which all fins produce is modeled below. Where N_{fins} is the number of fins and r is the moment arm from the rocket's center line.

$$M_{roll} = N_{fins}Lr \quad (26)$$

The opposing aerodynamic damping forces on the rocket fins are modeled as. Where C_{lp} is the rolling damping coefficient, d is the rocket diameter, and lastly V is the velocity of the rocket found from matlab 2 seconds after launch.

$$M_{damp} = -\frac{1}{2}\rho V d^4 C_{lp}\omega \quad (27)$$

The net torque required to reach and induce a z-axis roll to our desired roll rate.

$$M_{Net} = I_z\frac{\Delta\omega}{\Delta t} \quad (28)$$

The minimum amount of torque each fins must produce to induce a roll.

$$M_{tot} = M_{Net} + M_{damp} \quad (29)$$

The servo hinge moment, which will govern our servo motor selection and sizing.

$$M_{Hing} = qSCC_{h\delta}\delta \quad (30)$$

Equation Variables:

I_z: Axial mass moment of inertia
ω: Angular Velocity
M_{roll}: Rolling moment from fins
M_{damp}: Aerodynamic roll-damping moment
M_{Net}: Net torque to achieve target spin-up
M_{Hing}: Hinge moment

L: Lift Force
q: Dynamic pressure
S: Reference Fin area
$C_{c\alpha}$: Life curve slope per rad of angle of attack
$C_{h\delta}$: Control effectiveness
δ: Fin deflection/control surface

Two Fins	Altitude at deployment (Feet)	Max. Altitude (Feet)	Max. Velocity Miles/Hour	Time to Apogee (s)	Time to Burnout (s)	Velocity at deployment (Miles/Hour)
Small Fin	4140.67	4271.36	866.53	12.42	1.34	59.06
Medium Fin	429.62	1228.78	377.28	7.28	1.34	110.03
Large Fin	115.84	1006.5	326.34	6.71	1.34	112.55
Four Fins	**Altitude at deployment (Feet)**	**Max. Altitude (Feet)**	**Max. Velocity Miles/Hour**	**Time to Apogee (s)**	**Time to Burnout (s)**	**Velocity at deployment (Miles/Hour)**
Small Fin	321.26	1152.27	367.31	7.07	1.34	110.86
Medium Fin	239.03	1092.2	347.21	6.94	1.34	111.44
Large Fin	n/a	692.64	253.37	5.76	1.34	n/a

Table 1: Fin Statistics

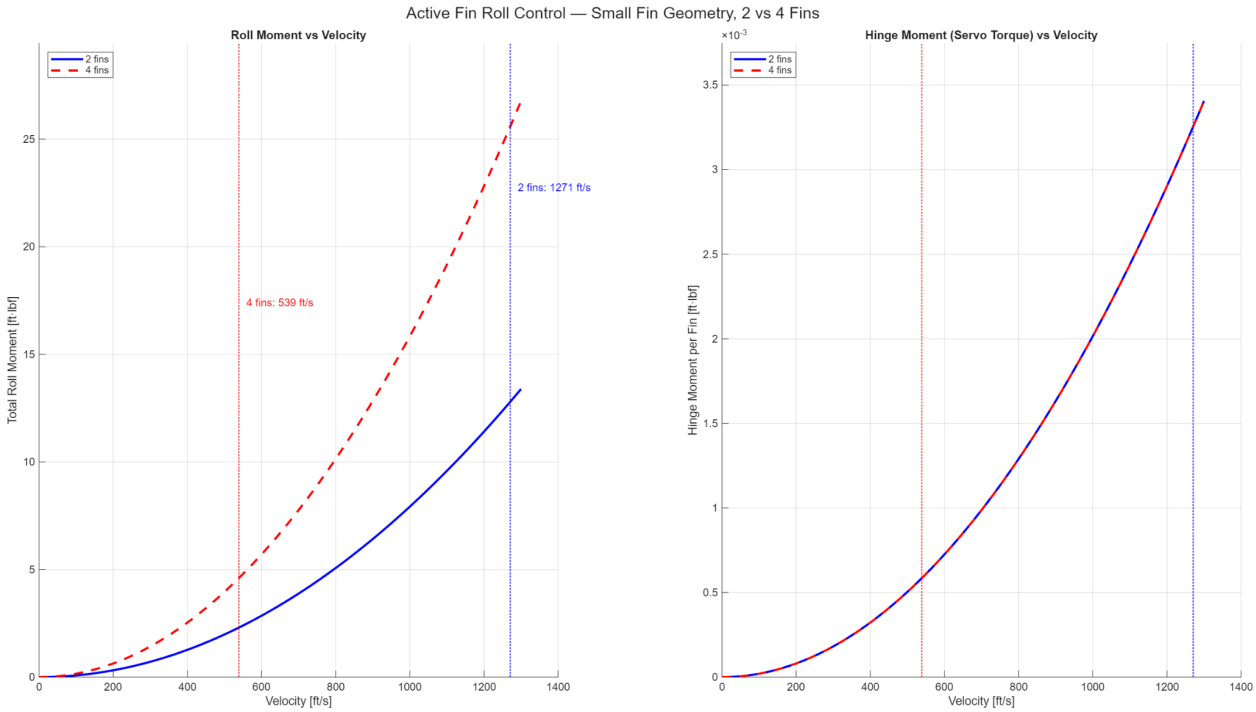

Figure 4: Active Fin Roll Control Graphs

The results of the following can be seen in the figure above, the one on the right being the comparison of roll moment vs velocity and the other Hinge moment vs velocity. As stated in the mathematical modeling section the velocity was found by simulating flights in rockism, where both fins were as tested as seen in table above. The table below also displays the results of the servo torque and fin moment modeling.

Roll Moment:	Hinge Moment:	Servo Torque:
Two Fins = 12.80 ft-lbf	Two Fins = 0.003 ft-lbf	Two Fins = 0.527 ft-lbf
Four Fins = 4.60 ft-lbf	Four Fins = 0.001 ft-lbf	Four Fins = 0.262 ft-lbf

Table 2: More Fin Statistics

The two-fin configuration produces higher roll moment, making it more effective for quickly reaching the 100 RPM spin rate. However, it requires the servo to produce 0.526 ft-lbf of torque.
The four-fin configuration produces less roll moment, requires less servo torque and improved roll damping. This leads to a smoother control and potentially smaller margin of error during flight. The additional fin also introduces aerodynamic drag which reduces maximum altitude and velocity but improves control authority.
Flight performance data reveal these trade-offs. A two-fin, small-fin configuration reached a deployment altitude of 4140.67 ft and a velocity of 866.53 mi/h, while the four-fin configuration reached 1152.27 ft and 367.31 mi/h under similar conditions. These results demonstrate that drag and mass penalties from additional fins can significantly affect apogee and flight time.

3.3.4 Center of Mass/Gravity & Stability

To determine the longitudinal stability of the rocket, three key aerodynamic parameters were calculated: the center of gravity (CG), center of pressure (CP), and stability margin (SM). These values form the foundation for evaluating static stability prior to flight simulation.

Center of Gravity (CG)

The center of gravity was calculated by summing the moments of each major component about the rocket's tip and dividing by the total mass:

$$X_{cg} = \frac{\sum m_i x_i}{\sum m_i} \tag{31}$$

[26]

Part	Mass (oz)	Distance from Tip (in)	(m_i x_i)
Nose Cone	5	4.6	23
Arduino Bay	0.88	15	13.2
Body Tube	13	29.88	388.4
Fins	2	43.25	86.5
Motor	9.81	44.75	439
Total	30.69	N/A	950.1

Table 3: Dimensional Assumptions

The **CG** location is measured at 30.96 in, which lies near the midpoint of the rocket body, aligning with expected stability characteristics for the Hi-Tech model dimensions (49.75 in total length).

$$X_{cg} = \frac{950.1}{30.69} = 30.96 \text{ in (from nose tip)}$$

Center of Pressure (CP)

$$X_{cp} = \frac{\sum (C_{N\alpha,i} \cdot l_i)}{\sum C_{N\alpha,i}} \quad (32)$$

[28]

The CP is determined from the weighted contributions of aerodynamic surfaces (nose cone, body, fins). This value will later be verified through Barrowman-based simulation and CFD analysis.

$$SM = \frac{X_{cp} - X_{cg}}{D} \quad (33)$$

[28]

A positive result between 1.0 and 2.0 calibers indicates adequate static stability. The ratio will confirm proper longitudinal balance once the pressure location is finalized.

The calculated center of gravity provides a baseline for further analysis. The remaining parameters will be used to complete the static stability assessment and verify that the design maintains aerodynamic control during flight.

3.3.5 Damping and Vibrations

To evaluate the vibrational response of the rocket's internal components, damping behavior was analyzed using two materials for comparison: PETG and Sorbothane. These calculations establish baseline transmissibility and damping ratios to understand how vibration energy is managed through the rocket's structure.

m	0.020 kg
k	5000 N/m
c_{PETG}	2 N*s/m
c_{Sorb}	10 N*s/m
$\omega_n = \sqrt{\frac{k}{m}}$	500 rad/s
$\omega_n = \sqrt{\frac{k}{m}}$	940 rad/s
$\zeta = \frac{c}{2\sqrt{km}}$	0.10 (PETG); 0.50 (Sorbothane)
$T = \frac{\sqrt{1+(2\zeta r)^2}}{\sqrt{(1-r^2)^2+(2\zeta r)^2}}$	0.58 (PETG); 0.19 (Sorbothane)

Table 4: Damping Variables Sorting for Calculations

Damping Ratios

Values of 2 N·s/m (PETG) and 10 N·s/m (Sorbothane) were used to represent low- and high-damping materials, respectively. The system parameters are summarized below.

$$\zeta = \frac{c}{2\sqrt{km}} \tag{34}$$

[33]

$$\zeta = 0.10\ (\text{PETG}),\ 0.50\ (\text{Sorbothane})$$

Natural Frequency

This represents how rapidly the system oscillates when displaced from equilibrium without damping effects. A higher natural frequency indicates a stiffer or lighter system that responds more quickly to external forces.

$$\omega_n = \sqrt{\frac{k}{m}} \tag{35}$$

[33]

Transmissibility

Transmissibility measures how much input vibration is passed through to the supported component. Lower values indicate greater isolation performance, meaning the material better absorbs vibration energy instead of transmitting it.

$$T = \frac{\sqrt{1 + (2\zeta r)^2}}{\sqrt{(1 - r^2)^2 + (2\zeta r)^2}} \tag{36}$$

[33]

T = 0.58 (PETG), 0.19 (Sorbothane)

With Sorbothane having a lower transmissibility, these calculations signify that this will be the better choice of material for damping when implementing the sensor housing/mounting.

3.3.5 Structural and Thermal Modeling

Structural Stress Analysis

The primary objective of the structural analysis was to verify that the 3D-printed PLA rocket body and avionics bay can withstand the mechanical and aerodynamic forces encountered during powered ascent. The analysis focused on the compressive and tensile stresses generated by thrust and drag at launch, using the AeroTech H55 motor (thrust = 113.3 N) as the primary load source.

The rocket body was modeled as a thin-walled cylinder with an outer diameter of 75 mm, inner diameter of 73 mm, and length of 1.2 m. The effective cross-sectional area was calculated as

$$A_c = \pi(r_{out}^2 - r_{in}^2) = 2.32 \times 10^{-4}\,\mathrm{m}^2 \tag{37}$$

The corresponding maximum compressive stress due to motor thrust was

$$\sigma = \frac{F}{A_c} = \frac{113.3\,\mathrm{N}}{2.32 \times 10^{-4}\,\mathrm{m}^2} \approx 4.88 \times 10^5\,\mathrm{Pa} = 0.49\,\mathrm{MPa} \tag{38}$$

Given that the yield strength of PLA is approximately σ_y=60 MPa, the calculated stress represents less than 1% of the allowable limit, confirming a substantial safety margin. The resulting compressive strain was computed as

$$\varepsilon = \frac{\sigma}{E} = \frac{4.88 \times 10^5}{3.5 \times 10^9} = 1.4 \times 10^{-4} \quad (39)$$

corresponding to an axial shortening of approximately 0.17 mm over the 1.2 m body length.
A supplementary aerodynamic load analysis was conducted for the nosecone using the drag equation

$$F_{dn} = \frac{1}{2}\rho V^2 C_D A \quad (40)$$

Assuming a subsonic velocity of $V = 52\ m/s$, air density $\rho = 1.18\ kg/m^3$, $C_D = 0.15$ (Haack-series profile), and a frontal area $A = 4.42 * 10^{-3}\ m^2$, the drag force was estimated as $F_{dn} = 1.06\ N$. This value confirms that aerodynamic drag loads are negligible compared to motor thrust, reinforcing the structural adequacy of the PLA airframe under expected flight conditions.

Avionics Bay Thermal Analysis
The avionics bay was thermally analyzed to evaluate the steady-state temperature rise due to internal electronics heat generation. Each design was modeled as a closed cavity with an internal power dissipation of $Q = 4\ W$ and external convection coefficient $h = 5\ W/(m^2 * K)$. The air properties were assumed as density $\rho = 1240\ kg/m^3$ and specific heat $c_p = 1800\ J/(kg * K)$. The steady state temperature was found from

$$\Delta T = \frac{Q}{hA} \quad (41)$$

$$T_s = T_\infty + \Delta T \quad (42)$$

where A is the external surface area of the bay. Two configurations were compared: Design 1 (four-rail harness) and Design 2 (two-rail + slab support). The measured surface areas ($0.0224\ m^2$, $0.0303\ m^2$, respectively), the predicted surface temperatures were found to be 70.7 °C and 61.4 °C, for the Four Rail vs Two Rail + Slab designs. Results show that Design 2 runs approximately 9 °C cooler due to the increased surface area and heat dissipation path. Even under worst-case ambient conditions (35 °C), both designs remain below the 70 °C softening point of PLA, confirming thermal stability for short-duration flights. However due to the short launch and motor burn time- extensive accumulation of heat over time is to be assumed near negligible.

The transient response was characterized by the thermal time constant

$$\tau = \frac{C}{hA} \quad (43)$$

Where $C = mc_p$ is the thermal capacitance of the printed structure. Calculations yielded time constants of 792 s and 727 s for Designs 1 and 2, respectively, indicating that the bay temperature approaches steady-state well after the rocket's total flight duration (<60 s).

---

4 DESIGN CONCEPTS - Henry Benedictus

4.1 Functional Decomposition

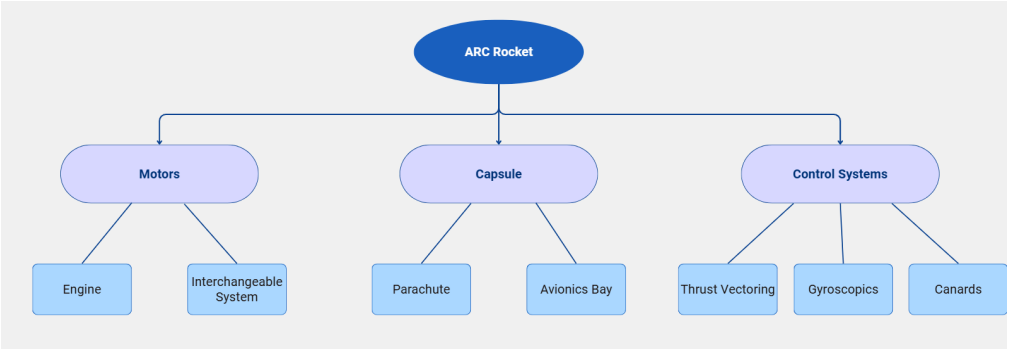

Figure 5: Functional Decomposition Chart

The Functional Decomposition shown in Figure 5, displayed the three main systems that are incorporated into the ARC Rocket. The first system is the rocket motor, which entails two different subsystems: the engine that will be used to propel the rocket to an appropriate height, with an appropriate time to apogee, and an interchangeable engine system to change the diameter of the rocket depending on future needs. The Capsule system is where the rocket will house the parachute for descent, and the modular avionics bay that will house all of the electronics and sensors. Finally, the Control Systems lays out three potential methods to induce a spin. The first being Thrust Vectoring, which incorporates compressed CO_2air, the second using a Gyroscope to induce a spin, and the last being canards at either the front or aft end of the rocket to control it. The importance of the chart is to easily separate the systems of the rocket to then easily separate work load among team members

.

4.2 Concept Generation

4.2.1 Motor Capsule

The motor for the rocket is to be placed in the aft part of the fuselage. For the project, single-use motors will be used, and thus need to be easily replaceable while also being held securely enough to not interfere with safety and performance requirements. Furthermore, size of motors can vary, so the specific capsule needs to accommodate the selected motor for the project. CAD was used in order to generate and design two different capsule variations.

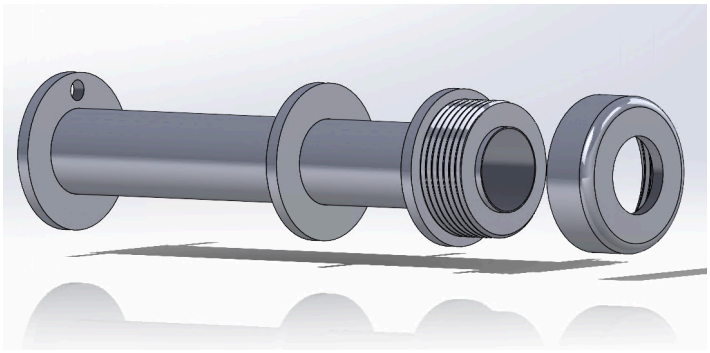

Figure 6: Motor Capsule Design 1

Method 1: Fixed Capsule.

This capsule fits one size of motor. The capsule would sit fixed at the base of the fuselage. The motor would be placed inside and replaced via the unscrewable top.

Advantages:

This capsule would require less parts and would be the easiest to assemble both as a part and into the rocket as a whole.

Disadvantages:

This capsule would not allow for a lot of interchangeability which would restrict us to one size of motor and be harder to maintain if the rocket sustains damage in any test flights.

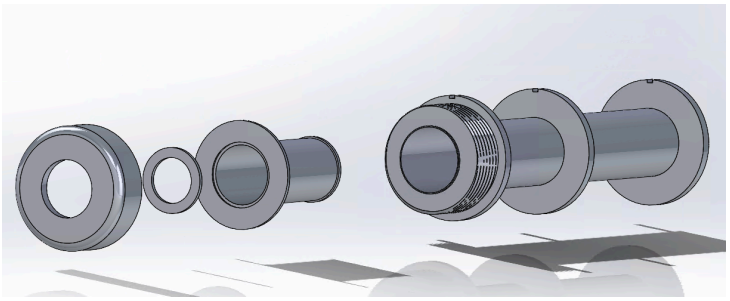

Figure 7: Motor Capsule Design 2

Method 2: Non-Fixed Capsule with Adapter

This capsule contains an adapter that can be inserted or removed in order to accommodate more than one size of motor. Furthermore, it is designed with notches for a slide bar inside the fuselage in order to slide it in and out of the body.

Advantages:

This capsule can be used to accommodate more than 1 size of motor giving us more room to experiment with motors of different dimensions. It also is removable for easy access in case of the need for maintenance.

Disadvantages:

This design would require more parts and it more complex in general. It is not needed if only one size of

motor is utilized for the duration of the project

4.2.2 Thrust Vectoring

Using air, the rocket can induce a spin with exit outlets that are parallel to each other on the rocket fuselage, pointing in opposite directions. To stop or prevent the rocket's spin, it will need to have another set of exit outlets pointing in the opposite direction from the other pair of outlets. A CAD model of this system is shown in Figure 7. Rockets naturally tend to spin during flight. Using the onboard flight computer, the appropriate outlets can be used to better induce the spin. There are two methods looked into to determine which one will be best.

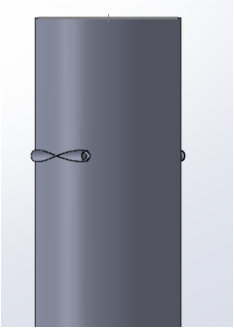

Figure 8: Exit Outlets for Thrust Vectoring

Method 1: Contained Compressed CO_2

Using compressed CO_2 canisters held within the main fuselage of the rocket. Using solenoids connected to the flight computer, it will eject the compressed air outside of the rocket to induce the spin. Using the flight computer, the fuel can be conserved during bursts of air versus a heavy steady flow. A image of concept is shown in figure 8.

Advantages:

The biggest advantage of using internally stored compressed CO_2 is that the air pressure can be easily predicted through mathematical modeling since it is a controlled system. The air container could also be easily adjustable for the needs of future launches.

Disadvantages:

Using an onboard air cartridge will significantly increase the weight of the rocket, which in turn changes the center of mass and pressure, while also requiring a larger motor, which can increase the cost of the launch.

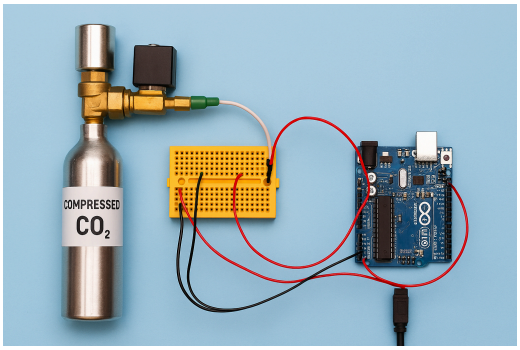

Figure 9: Concept Generation of Solenoid Connected to Arduino

Method 2: Redirecting Air Through the Nose Cone

Using the air that the rocket goes through while in flight, the idea is to have inlet holes within the nose cone, and using solenoids to let air be redirected through the sides. A image of design of concept can be shown within figure 10.

Advantages:

By redirecting the air from the nose cone, there isn't a need to house an internal compressed capsule, thus making it much lighter than Method 1.

Disadvantages:

After the motor fully burns, it will start to decelerate due to gravity. This means that the velocity of the incoming air at the nose cone will significantly decrease within the time to apogee. This isn't suitable to bring the rocket to the necessary angular velocity and bring it to a stop within the time of flight.

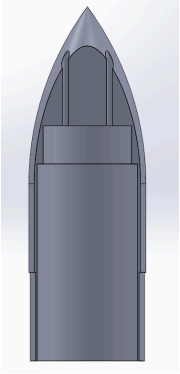

Figure 10: Inlet Holes for Method 2

4.2.3 Active Aerodynamic Fins

The active fin concept includes an active frontal canard system, which are separated into two subsystems, one being two fins and the other being four fins. Each concept generated was evaluated on aerodynamic performance, control authority, and over stability.

Method One: Two Active Canards

This configuration uses two active canards near the payload section of the rocket body, symmetrically mounted.

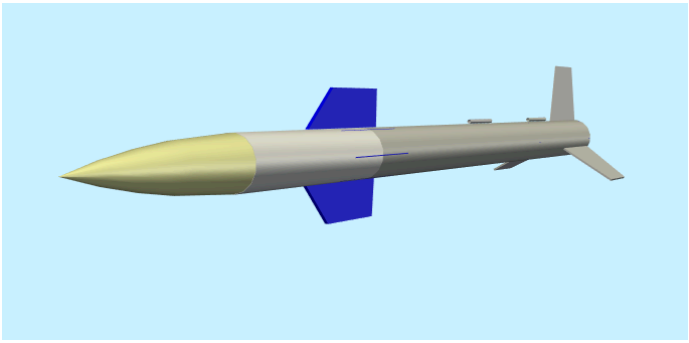

Figure 11: Two Active Canards

Advantages:

Some advantages of the two fin system is that it has a lower overall system weight compared to other control methods, with improvement to thrust to weight ratio. This concept also contributes to a lower amount of drag on the fin surface resulting in higher velocity and greater altitude. Additionally only two server motors are required to control this concept.

Disadvantages:

Some disadvantages would be a lower control authority over this concept's control system, since the system would produce less aerodynamic force, limiting the roll correction. A slower dynamic response would also occur since adjustment to roll would be more gradual which would affect stability and delay the system to reach 100 RPM.

Method Two: Four Frontal Active Canard

This configuration uses four active fin mounted evenly around the rocket body.

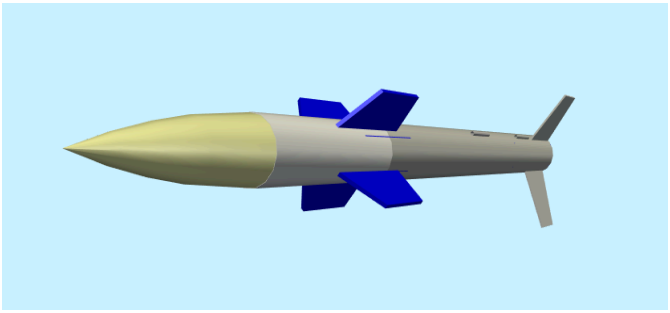

Figure 12: Four Active Fins

Advantages:

Some advantages would be a higher control authority, since the rocket can generate more precise aerodynamic forces. An improved reliability would be present, since there would be redundancy, which reduces the risk of failure of one server motor.

Disadvantages:

Some disadvantages would be the increase of mass within this configuration, with the additional increase of drag along the rocket body and fin surface. These would results in a lower apogee and a shorter flight time, affecting our ability to induce a roll, and potentially affect flight performance. This configuration also has a higher stability margin, which is typical beneficial, but can limit maneuverability and responsiveness.

4.2.4 Gyroscope Sensor Dampening Housing/Mounting System

To ensure reliable IMU readings during flight, a modular mounting system was developed for the gyroscope and accelerometer sensor. The primary goal of this subsystem is to isolate the ICM-20948 (or equivalent) from excessive vibration, thereby reducing noise in the sensor data and improving closed-loop stability for the control algorithm.

Two initial designs were created for this subsystem, each prioritizing different aspects of manufacturability, damping, and heat resistance. Both were modeled in SolidWorks for fit within the avionics bay and analyzed alongside the damping vibration study from Section 3.3.5.

Assumptions

- Sensor mass and geometry were modeled based on the ICM-20948 development board.
- Material properties for Sorbothane and PETG were taken from manufacturer data used in Section 3.3.5.
- Mount stiffness and damping were approximated as a single-degree-of-freedom system representing the dominant vibration mode in the avionics bay.
- Adhesion points were assumed sufficient for loads below 70 lbf as defined in Engineering Requirement ER-6.

Design 1: PA12 (Nylon) and Sorbothane Hybrid

This design uses a two-material configuration consisting of a rigid nylon shell to provide structural support and a Sorbothane insert to absorb high-frequency vibrations. The internal Sorbothane layer surrounds the gyroscope housing, reducing vibrational transmission from the rocket body to the sensor. The hybrid nylon-Sorbothane configuration was selected for further prototyping due to its superior damping behavior and potential to reduce signal noise from mechanical vibrations. Although PETG provides better manufacturability, its low damping limits its effectiveness for flight data accuracy. The chosen design will undergo further testing to validate the damping model and verify that the sensor's output remains within the required error margin for z-axis roll measurements.

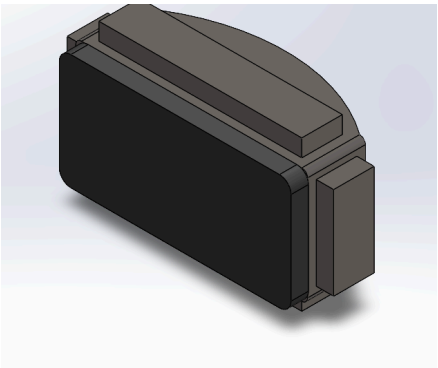

Figure 13: Sorbothane Sensor Housing

Advantages:

This design provides high vibration isolation thanks to the elastic Sorbothane layer, which effectively dampens transmitted vibrations to the IMU module. It also maintains strong mechanical protection for the sensor, ensuring structural integrity during launch and recovery. Additionally, the modular insert design allows for easy sensor replacement without the need to reprint the entire housing, improving serviceability and testing flexibility.

Disadvantages:

However, the design requires precise manufacturing and bonding of two materials, which increases production complexity. It also adds extra mass compared to a simpler, single-material mount. Lastly, additional adhesive or fastener points may be necessary to prevent detachment under high load conditions, introducing further assembly considerations.

Design 2: PETG

The second concept employs a simpler one-piece PETG mount. PETG provides adequate stiffness and temperature resistance while remaining easy to print and replace. This design sacrifices some damping performance but offers improved manufacturability for early testing phases.

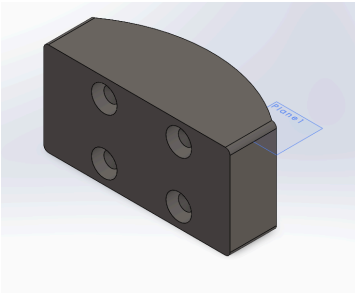

Figure 14: PETG Sensor Housing

Advantages:

This design is easy to manufacture and replace using FDM 3D printing, allowing for quick prototyping and iteration. It offers high thermal resistance, making it suitable for flight environments where temperature fluctuations are common. The lightweight and compact structure also minimizes added mass, which is beneficial for maintaining overall rocket performance.

Disadvantages:

On the other hand, it provides limited vibration isolation due to its low damping properties, which can allow unwanted vibrations to reach the IMU. This may result in the transmission of high-frequency noise to the sensor, potentially reducing measurement accuracy. Additionally, the design is less effective for precision roll control testing, where fine vibration filtering is critical.

4.2.5 Avionics Bay and Electrical Harness

The avionics bay serves as the central compartment for housing all electrical and control components of the Active Rocket Controls (ARC) system. Two primary concepts were generated for this subsystem, each offering distinct advantages for modularity, thermal management, and ease of assembly.

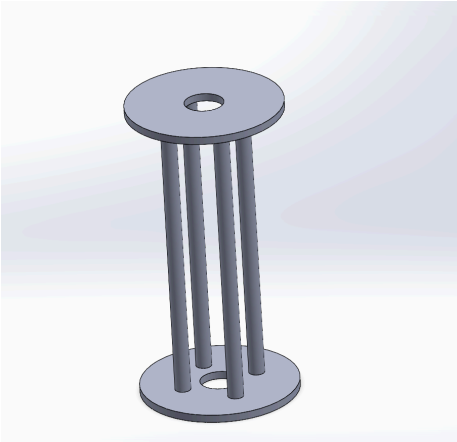

Figure 15: Four Rail Harness

Design 1 “Four Rail Harness”

This design prioritizes modular flexibility, allowing multiple electronic components (Arduino, IMU, data logger, power supply) to be reconfigured depending on mission requirements. The structure was designed from polylactic acid (PLA) using additive manufacturing to provide rigid mounting while maintaining a lightweight profile. This approach grants a higher degree of mounting freedom and potential stability due to distributed load paths across four mounting rails.

Advantages:

- Enables easy component swaps and rapid prototyping

- Provides Structural redundancy and improved alignment control

Disadvantages:

- Potential for localized heat accumulation from electronics

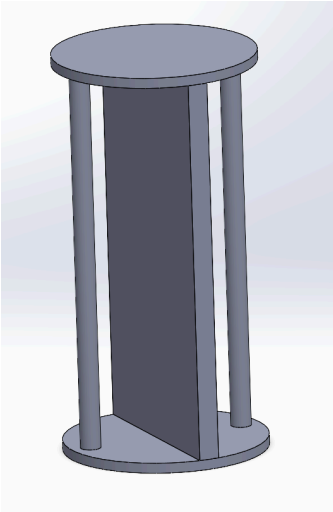

Figure 16: Two Rail + Slab Harness

Design 2 “Two Rails + Wall”

This configuration uses a simpler two-rail design integrating a slab-style mounting plate that spans the internal diameter of the bay. While offering fewer customization options, this design minimizes part count and reduces weight. Furthermore, the solid base improves thermal conduction to the external wall, reducing localized overheating within the avionics housing.

Advantages:
This design reduces thermal risk by allowing heat to conduct efficiently through the solid base, minimizing hotspots within the avionics bay. Its simplified layout also makes assembly easier and improves manufacturability, requiring fewer parts and less alignment precision during installation.

Disadvantages:
The added wall structure can result in slightly higher weight compared to fully open-frame configurations. Additionally, the reduced number of mounting points limits flexibility when positioning or swapping electronic components, making it less adaptable for future system modifications.

A comparative analysis between both configurations was later verified through structural and thermal modeling (Section 3.3.5), showing that the two-rail slab system maintained temperatures up to 9 °C cooler than the four-rail configuration at localized harness spots. Since motor burn time is expected to be extremely quick with local electronics heat transfer assumed to be negligible, we will move forward with the proposed “Four Rail” system due to its harness customization potential.

4.3 Selection Criteria

4.3.1 Engine Selection:

When selecting an engine that will be used for the launch, the simulation engine, RockSim, was used. An initial model file of a High-Tech rocket was chosen to be uploaded into RockSim since it is a similar-sized rocket that will be used. The file was found within the Apogee website, which produces the rocket and distributes other parts like the rocket motor [34]. RockSim has an internal database of usable motors for each model they have available, and can run multiple simulations with each motor, and determine whether or not it will produce a safe flight. With this, multiple simulations were used to determine which motor would be best suited for the project. Starting from 0 additional pounds to 4 additional pounds. After weeding out the motors to the ones that cannot safely launch 4 lbs, further information was extracted from the ones that can. The results are shown within Table 5.

Motor Type	Velocity at Departure (mph)	Thrust to Weight	Max Y Accel (Gs)	Max Velocity (mph)	Max Altitude (Ft)	Time to Apogee (Sec)
[H219T]	29.6847	10.828	22.2	180.1255	1120	8.6252
[H283ST]	31.84	12.551	28.153	155.59	841.87	7.459
[H550]	45.5979	24.378	23.864	254.556	1915.6	10.825
[I500T]	39.1465	18.493	19.129	448.476	4759.55592	16.249
[I175WS]	27.3056	9.527	10.414	223.4377	1936.78813	11.441
[I350]	35.0029	14.796	16.031	457.049	4948.29	16.964

Table 5: Motor Data That Can Withstand an Extra 4 lbs

Based on the data from Table 5, it was decided to purchase two I500 38mm motors for the anticipated launches since it gives an approximate 16 seconds to apogee, which is the longest available time to induce the rocket roll. The reason why the I500T was chosen over the I350, which outperforms it a little, is because it was $30+ per motor compared to the I500T. For the test in November, a standard H100 motor will be used since it is affordable and is strong enough to launch a light payload of sensors for the initial test.

4.3.2: Material Selection

Two materials will be primarily used throughout the rocket design. The first material will be fiberglass for the fuselage and capsul, because it is much stronger and lighter than using either cardboard or polylactic acid filimant (PLA). The main part that is made out of fiber glass will be the rocket fuselage since it will be undergoing the majority of the forces and can be easily modified without changing the structural integrity.

PLA will be used however when creating smaller internal components, due to the fact that it is much easier to produce than fiber glass parts. The parts that they will be used for will be goeing through multiple iterations, and will be much cheaper to use just PLA for these parts.

For the first test, the main materials that will be used is cardboard and craft wood since the flight will use an already existing rocket platform, with a PLA printed capsule.

Figure 17: Example of Fiber Glass Rocket Parts [42]

4.3.3: Eletrical Engineers Parts

The electrical engineering team have ordered sensor parts, and audruinos that will be used within the first test launch. These parts will eventually be used to control the rocket with the chosen system at the second test lauch later in Spring 2026.

4.4 Concept Selection

Criteria	Weight	Thrust Vector Control	Active Fins	Mass Balance Gyroscope	Modular Avionics Bay system	Motor Mount	Average
Cost	25%	3	3	5	3	4	3
Mass	15%	2	2.5	4	3	5	3.3
Reliability	10%	4	2	5	5	4	4
Stability	15%	5	3	1	5	5	3.8
Control (Roll)	20%	2	5	1	5	5	3.6
Manufacturability	15%	4	4	4	4	4	4
TOTAL	100%	3.2	2.815	1.975	3.175	3.65	6.49

Table 6: ARC Decision Matrix

When deciding which system to use, the group collaboratively created the Decision Matrix shown in Table 6. Weighing the importance of each criteria which totaled 100%. The group discussed each of their own chosen systems and weighed them accordingly. The most important was cost since the project has a limited budget. Control is how well each active control unit will induce the roll for the rocket. This was the second most important because if it cannot control the rocket well, the target goal will not be reached. Stability in the flight is how stable the control system is, the lower the score the less stable it is determined to be. Stability is important because it can determine how safe each method is. The more mass within the rocket system, the less time it has to be able to induce the roll since it will reach apogee faster, and have a lower velocity after the motor burns out. Since a majority of the rocket's frame, and internal systems will be manufactured by the team, it is important that each system is easily manufacturable, and not too complex which can in turn make it harder to manufacture. Finally the system has to be reliable. If it doesn't work well, or is too complex, it is counted against the reliability, since more can go wrong.

When calculating the scores, each system was graded from 1-5 for each criteria, with 1 being the lowest score, and 5 being the highest score. From there, the total score for each system was totaled by multiplying the score associated with its criteria, and adding them all together. The average score was also found for each criteria by adding the scores and dividing it by 5 (since there are 5 systems graded). After grading all systems, the control system chosen was the Thrust Vector Control Unit with a score of 3.2, and the backup control system is the canards with a score of 2.815. The group decided to have a back system just in case the system that is researched and worked on ends up not working when building it or if something goes wrong in the design process.

Once all of the systems were chosen, the group created a CAD model within SolidWorks which can be shown in Figure 18, with its corresponding Bill of Materials (BOM) in Figure 18.

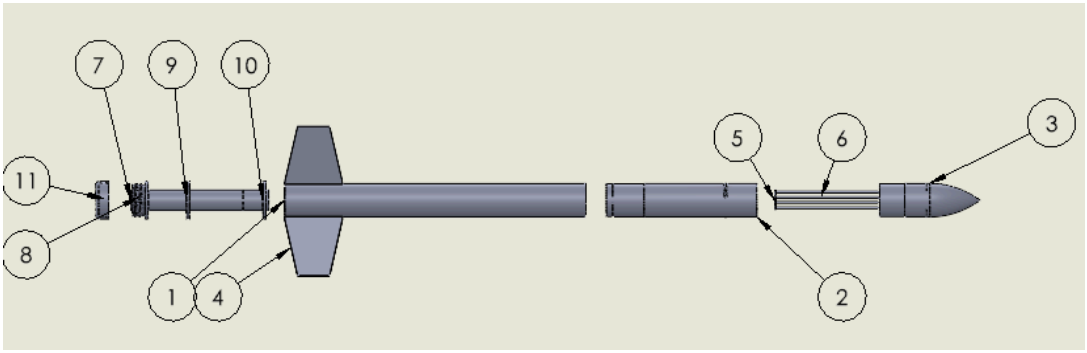

Figure 18: ARC Exploded View

BOM Table			
ITEM NO.	PART NUMBER	DESCRIPTION	QTY.
1	Rocket_Fusaloge_1.0		1
2	Rocket_Capsole_With_Exit_Holes_1.0		1
3	Rocket_Nose_Cone_#1		1
4	Rocket_Base_Fin_1.0		3
5	Base_Ring_For_Capsule		2
6	Base_Ring_Rod		4
7	capsule		1
8	ScrewHub		1
9	RingFIXED		2
10	RingFIXED2		1
11	Cap		1

Figure 19: ARC Bill of Materials Associated with Exploded View

In the future, the BOM will progressively increase in item number. Figure 18 is simply a rough estimate of what will be incorporated into the ARC. It doesn't include nuts and bolts that will be needed to secure the Base Rings and Rods for the modular housing capsule, any electronic components used by the Electrical Engineers, or all the components for the control system.

5 CONCLUSION - Emilio Huggins

The Active Rocket Controls (ARC) project focused on designing and developing a high-powered, level-one rocket with active roll stabilization about its longitudinal z-axis. The goal was to demonstrate controlled roll induction and damping through an integrated feedback system while staying compliant with Tripoli Rocketry Association safety and competition standards. The main project priorities were stability, manufacturability, cost efficiency, and reliability during both launch and recovery.

Throughout the semester, the team followed a structured engineering design process that began with system-level benchmarking of control methods used in aerospace applications, including aerodynamic canards, thrust vector control, and mass-momentum shifting systems. After evaluating these concepts through a weighted decision matrix, thrust vector control was selected as the most practical and scalable approach for achieving precise roll control at the model-rocket scale.

Subsystem-level benchmarking and modeling supported this decision. The avionics bay and fin control system were developed through iterative design and analysis. Two avionics bay configurations were explored: a modular four-rail “freedom harness” and a simplified two-rail slab design. Each option was evaluated for thermal management, mass, and ease of access. The four-rail configuration was ultimately chosen because it offered the most flexibility for customization. Similarly, two active canard configurations were compared to balance control authority, drag, and mechanical reliability. The final selection was a two-servo canard setup that provided simple operation and effective roll performance.

In parallel, the team performed literature reviews, structural and thermal modeling, and preliminary simulations to confirm feasibility. These studies showed that the final subsystem designs meet the project’s performance goals and remain within material and operational limits. The combination of open-source electronics, additive manufacturing, and validated control modeling creates a solid foundation for future development.

By the end of the semester, the ARC team had completed a conceptual design that integrates aerodynamic roll control with modular avionics and a strong structural framework. The result balances innovation with practicality and supports the educational goals of the project. Moving forward, the team will begin prototyping, hardware integration, and closed-loop testing to prepare for full-scale flight demonstrations later in the semester.

6 REFERENCES

[1] Tripoli Rocketry Association, *"Unified Safety Code,"* 2025. [Online]. [Accessed: Sep. 08, 2025].

[2] Apogee Components, Inc., *"Peak of Flight Newsletter: When the Data Goes Sideways: Why Your Rocket's Descent Position Might Be Wrong,"* 2023. [Online]. [Accessed: Sep. 08, 2025].

[3] M. R. Spakovszky, *Thermodynamics and Propulsion,* MIT Unified Engineering Notes, 2025. [Online]. [Accessed: Sep. 08, 2025].

[4] AIAA OC Rocketry, *"Arduino Tutorials,"* 2025. [Online]. [Accessed: Sep. 09, 2025].

[5] Apogee Rockets, *"RockSim Information,"* 2025. [Online]. [Accessed: Sep. 10, 2025].

[6] P. Moschidis and P. S. Bithas, *"Arduino Rocket Flight Computer,"* in *Proc. PACET,* pp. 1–6, Dec. 2022, doi: 10.1109/pacet56979.2022.9976324.

[7] Dejan, *"Arduino and MPU6050 Accelerometer and Gyroscope Tutorial,"* 2019. [Online]. [Accessed: Sep. 10, 2025].

[8] W. D. Wassgren, *"Compressible Flow – Converging Nozzle Reading,"* Purdue Univ., ME 30800 Notes, [Online]. [Accessed: Sept. 25, 2025].

[9] N. Nykanen, *"Basics of Angular Acceleration and Rotational Moment of Inertia,"* R+W America Blog, 2019. [Online]. [Accessed: Oct. 03, 2025].

[10] F. M. White and H. Xue, *Fluid Mechanics,* 9th ed., New York, NY, USA: McGraw-Hill, 2021. [Accessed: Sept. 29, 2025].

[11] S. Ainsworth, *"A Guide to Optimal Altitude: Part 2,"* Apogee Rockets Newsletter, 2015. [Online]. [Accessed: Sep. 14, 2025].

[12] G. P. Sutton and O. Biblarz, *Rocket Propulsion Elements,* 9th ed., Hoboken, NJ, USA: Wiley, 2017.

[13] Tripoli Rocketry Association, Inc., *"NAR-TMT Combined Motor List,"* 2025. [Online]. [Accessed: Sep. 14, 2025].

[14] AeroTech Consumer Aerospace, *"AeroTech Master Motor Matrix,"* updated Apr. 2, 2023. [Online].

[15] NASA Glenn Research Center, *"Specific Impulse" and "Rocket Thrust Summary,"* 2025. [Online]. [Accessed: Sep. 15, 2025].

[16] S. Bundalevski, V. Cingoski, and S. Gelev, *"Determination of the Total Impulse of the Solid Rocket Motor by Using Two Mathematical Methods,"* in *Proc. IT (SPIT),* 2018, pp. 1–3, doi: 10.1109/SPIT.2018.8350456.

[17] A. Praveen et al., *"Thrust Vector Control of Solid Propellant Model Rocket,"* in *Proc. INCOFT,* 2023, pp. 1–6, doi: 10.1109/INCOFT60753.2023.10425646.

[18] *RocketPy Documentation, "Roll Equations for High-Powered Rockets,"* 2025. [Online].

[19] R. Nakka, *"RD_fin — Rocket Fin Design and Aerodynamics,"* 2025. [Online].

[20] NASA, *The Practical Calculation of Aerodynamic Characteristics of Slender Finned Vehicles,* 1967 (Barrowman Report).

[21] *"Introduction to Rocket Design,"* 2025. [Online].

[22] *"An Actively Stabilised Model Rocket,"* Research Paper, 2025.

[23] J. D. Anderson, *Fundamentals of Aerodynamics,* latest ed., New York, NY, USA: McGraw-Hill.

[24] *"Design of a Servo Mechanism for Controlling Missile Fins in Pitch and Yaw Planes,"* Research Paper.

[25] *"Model Rocket Guidance by Canards,"* Research Paper.

[26] NASA Glenn Research Center, *"Rocket Center of Gravity,"* Beginner's Guide to Aeronautics, 2025. [Online].

[27] T. Van Milligan, *Numeric Methods in Model Rocket Design,* Apogee Rockets, Tech. Pub. #17.

[28] T. Van Milligan, *"How to Find the Center of Pressure on a Rocket,"* Advanced Construction Video, Apogee Rockets.

[29] ESRA, *International Rocket Engineering Competition Rules and Requirements,* ver. 1.6, 2025. ~Engineering Standard.

[30] G. Solomon and Y. Abreham, *"Analytical Calculation on Rocket Stability,"* Int. J. Res. Anal. Reviews, vol. 7, no. 3, 2020.

[31] R. Cadamuro, M. P. Cardillo, and L. F. Macaluso, *"A Static Stability Analysis Method for Passively Stabilized Sounding Rockets,"* Aerospace, vol. 11, no. 3, p. 242, 2024.

[32] J. Barrowman, *"TIR-33: Calculating the Center of Pressure of a Model Rocket,"* Nakka-Rocketry, [Online].

[33] A. Downey, *Vibration Mechanics: A Practical Introduction,* Clemson (SC): SC University Publications. [Online].

[34] *"Compression Tests of Tubing Used in Rocketry,"* Newsletter.

[35] *"Unified Analysis of Aerospace Structures through Implementation of Rapid Tools into a Stress Framework,"* Technical Report.

[36] *"3D Printing Temperature: Effects, Materials and Considerations,"* Technical Guide.

[37] *"Structural Design and Analysis of High-Powered Model Rockets Using OpenRocket,"* Journal.

[38] R. Nakka, *"Nosecone Design,"* Technical Tutorial.

[39] *"Reaction Wheel Based Rocket Active Spin Stabilization,"* Research Paper.

[40] *"Introduction to Rocket Design 9. Recovery System,"* Technical Tutorial.

[41] *"Hi-Tech,"* Apogee Rockets, Skill Level 3 Kit, [Online]. [Accessed: Oct. 10, 2025].

[42] *"Fiberglass Nose Cones,"* Mach 1 Rocketry, [Online]. [Accessed: Oct. 20, 2025].

7 APPENDICES

7.1 Appendix A: System QFD

System QFD — **Date:** September 2925

1	Weight Contraint									
2	Constrained Diameter		-9							
3	Z-axis Roll Orientation Error		9	-3						
4	Decrease control latency		9	-3	9					
5	Dynamic loading		-9	-3	3	9				
6	Reliablity		-3	-1	9	-9	9			
7	Cost		9	3	-3	-3	-9	-3		
8	with minimum 50% 3d printed custom parts		9	3	3	3	-3	3	3	
9	Fly Sheet Check		9	3	9	9	3	9	-1	9

Legend	
A	AIM-9X Sidewinder
B	Spacex Falcon 9
C	Blue Origin New Shepard

			Technical Requirements									Customer Opinion Survey				
	Customer Needs	Customer Weights	Weight Contraint	Constrained Diameter	Z-axis Roll Orientation Error	Decrease control latency	Dynamic loading	Reliablity	Cost	Consturct with minimum 50% 3d printed custom parts	Fly Sheet Check	1 Poor	2	3 Acceptable	4	5 Excellent
1	Dynamic z-axis control	8	3		9	9	3	3	1	3	9			A		BC
2	Fits 2.5-4" rocket body	4		9					3	9		ABC				
3	Demo launches	7			3		3	9	1	3	9			ABC		
4	Real-Time Feedback	1	1		9	9		3	1	3	9					ABC
5	Functions: No roll & Induced roll	6			3	3		3		1				C	B	A
6	Comply with Tripoli safety requirement	9		3	3	3	9	9	1	3		A	B	C		
7	Cost effective solution	3	1		1	1	1	3	9	9	1	ABC				
8	Inlcude 3D printed/custom parts	5		9	1	1		3	9	9	1	ABC				
9	Delvierables	2			3		3	9	9	9	9			ABC		
	Technical Requirement Units		lb	in	degree RPM	ms	lbf	%	$	n/a	n/a					
	Technical Requirement Targets		≤10lb	2.5-4"	2°, 100 RPM	≤50 ms	70	99%	$2,000	n/a	n/a					

7.2 Appendix B: Visualization of Formulas (1), (2), (3), and (4)

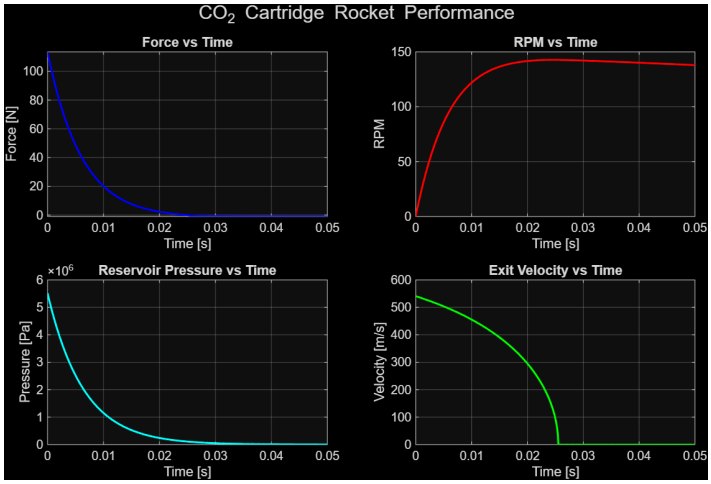

7.3 Appendix C: ***Thermal Resistance***

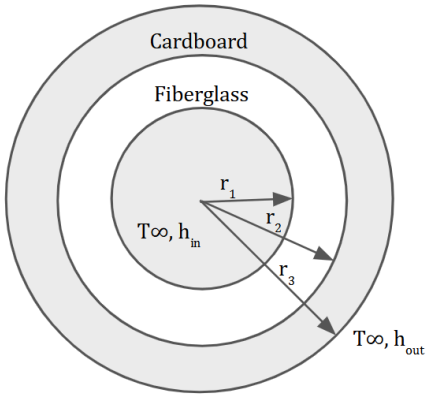

7.4 Appendix D: Fin Statistics

Two Fins	Altitude at deployment (Feet)	Max. Altitude (Feet)	Max. Velocity Miles/Hour	Time to Apogee (s)	Time to Burnout (s)	Velocity at deployment (Miles/Hour)
Small Fin	4140.67	4271.36	866.53	12.42	1.34	59.06
Medium Fin	429.62	1228.78	377.28	7.28	1.34	110.03
Large Fin	115.84	1006.5	326.34	6.71	1.34	112.55
Four Fins	**Altitude at deployment (Feet)**	**Max. Altitude (Feet)**	**Max. Velocity Miles/Hour**	**Time to Apogee (s)**	**Time to Burnout (s)**	**Velocity at deployment (Miles/Hour)**
Small Fin	321.26	1152.27	367.31	7.07	1.34	110.86
Medium Fin	239.03	1092.2	347.21	6.94	1.34	111.44
Large Fin	n/a	692.64	253.37	5.76	1.34	n/a

7.5 Appendix E: Active Fin Roll Control Graphs

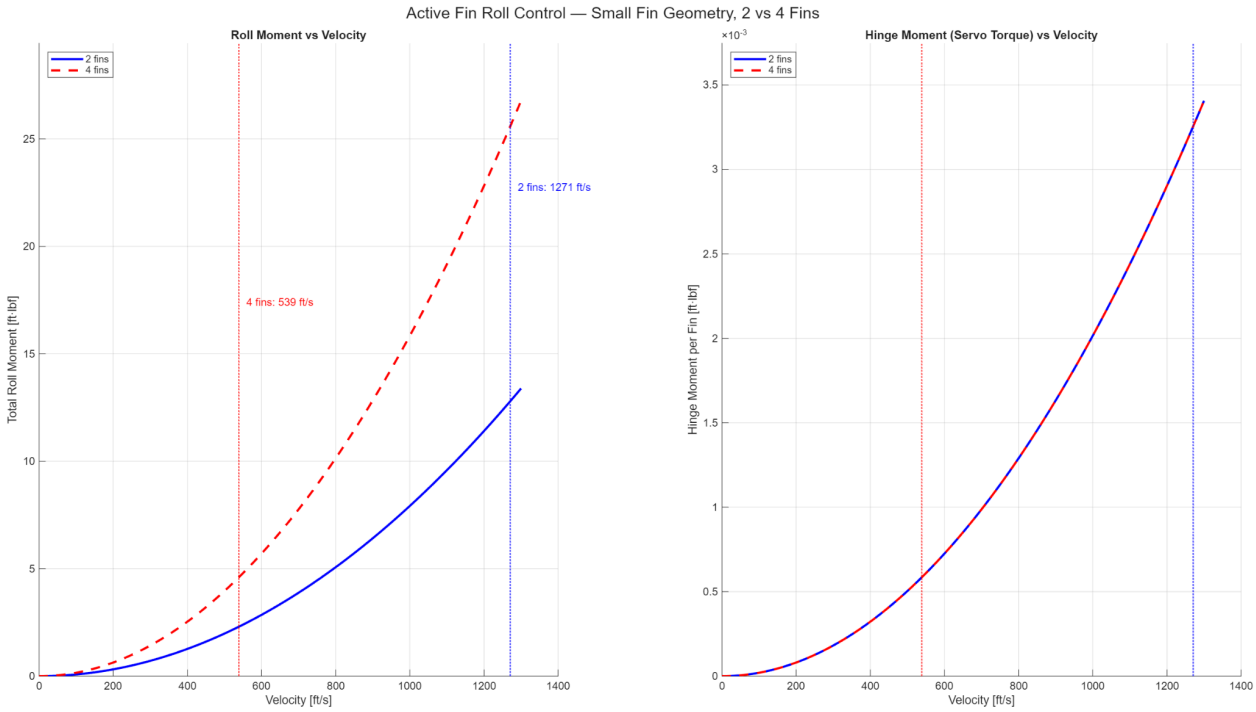

7.6 Appendix F: Functional Decomposition Chart

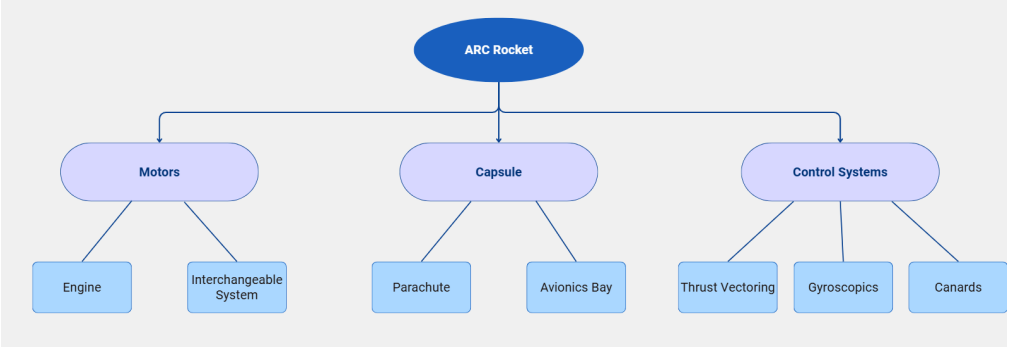

7.7 Appendix G: Motor Capsule Design 1

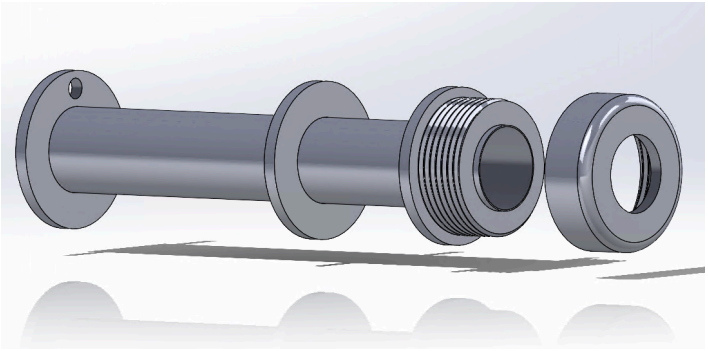

7.8 Appendix H: Motor Capsule Design 2

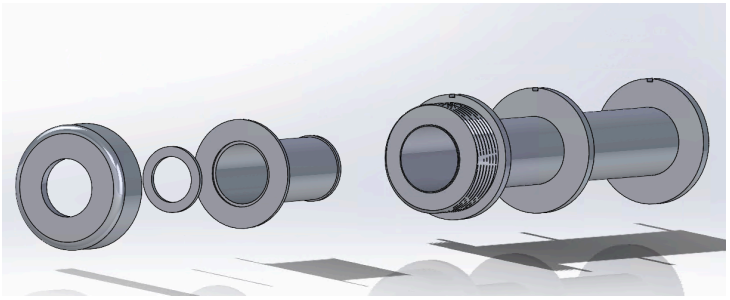

7.9 Appendix I: Exit Outlets for Thrust Vectoring

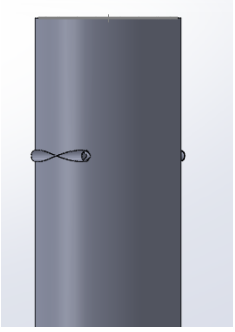

7.10 Appendix J: Concept Generation of Solenoid Connected to Arduino

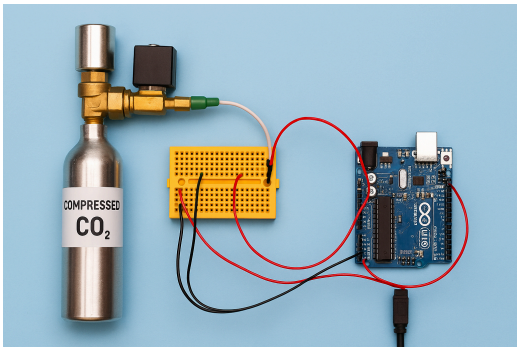

7.11 Appendix K: Inlet Holes for Method 2

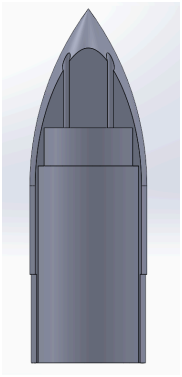

7.12 Appendix L: Two Active Canards

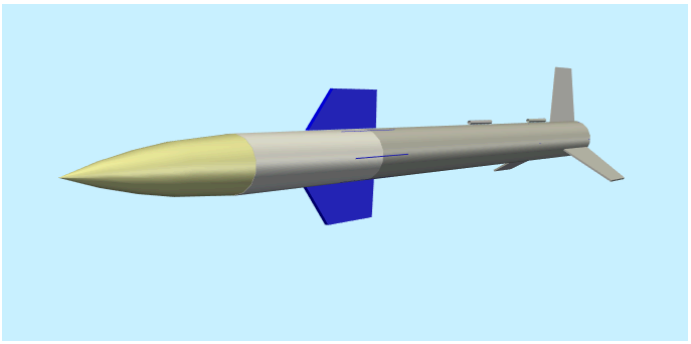

7.13 Appendix N: Four Active Fins

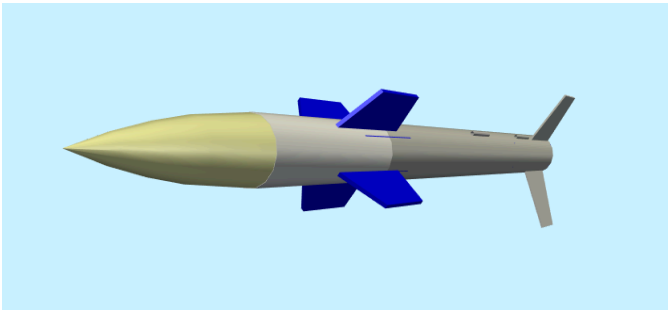

7.14 Appendix M: Sorbothane Sensor Housing

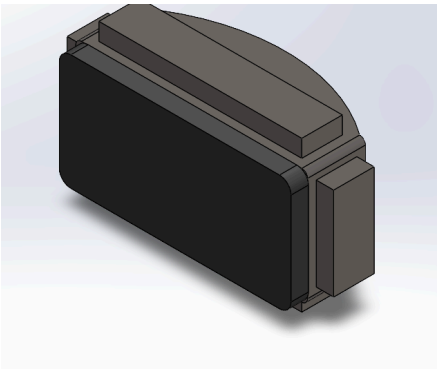

7.15 Appendix O: PETG Sensor Housing

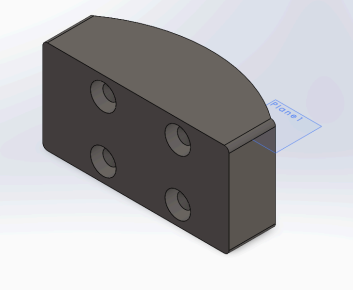

7.16 Appendix P: Four Rail Harness

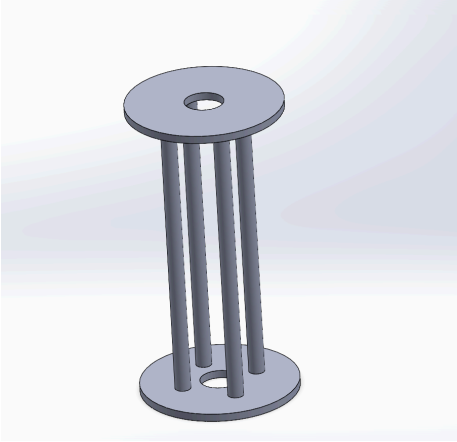

7.17 Appendix Q: Two Rail + Slab Harness

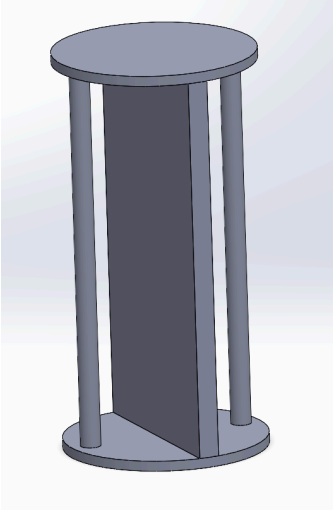

7.18 Appendix R: Example of Fiber Glass Rocket Parts

7.19 Appendix S: ARC Exploded View

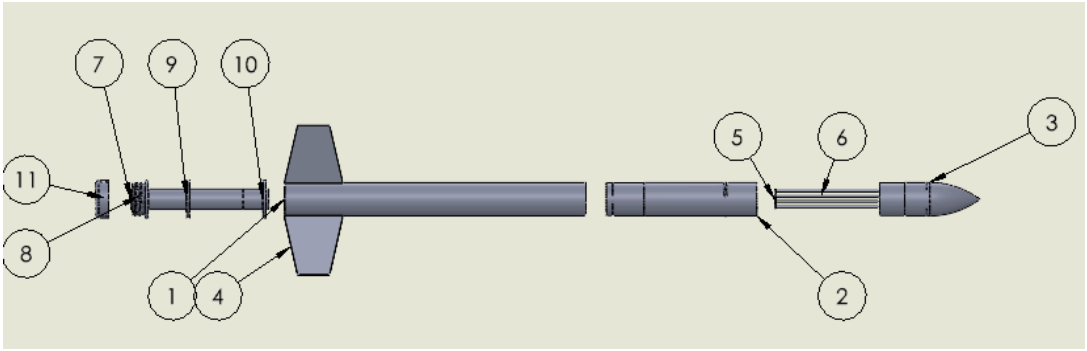

7.20 Appendix T: ARC Bill of Materials Associated with Exploded View

BOM Table			
ITEM NO.	PART NUMBER	DESCRIPTION	QTY.
1	Rocket_Fusaloge_1.0		1
2	Rocket_Capsole_With_Exit_Holes_1.0		1
3	Rocket_Nose_Cone_#1		1
4	Rocket_Base_Fin_1.0		3
5	Base_Ring_For_Capsule		2
6	Base_Ring_Rod		4
7	capsule		1
8	ScrewHub		1
9	RingFIXED		2
10	RingFIXED2		1
11	Cap		1

7.21 Thrust Vectoring Matlab

```
clear; clc; close all;
% --- Parameters ---
P0   = 861845;        % Initial reservoir pressure [Pa]
Pa   = 1.01325e5;      % Ambient pressure [Pa]
Ae   = 0.0003144;         % Exit area [m^2]
gamma= 1.289;          % Ratio of specific heats
R    = 188.92;         % Specific gas constant for CO2 [J/kg-K]
T0   = 293.15;         % Stagnation temperature [K]
V    = 0.00059;         % Reservoir volume [m^3]
M    = 2.942;          % Mass of rocket (kg)
r1   = 0.02889;        % Radius 1 of rocket (m)
r2   = 0.032512;       % Radius 2 of rocket (m)
% --- Derived constants ---
beta = (2/(gamma+1))^(gamma/(gamma-1));   % exit pressure ratio
K    = Ae*sqrt(gamma/(R*T0))*(2/(gamma+1))^((gamma+1)/(2*(gamma-1)));
lambda = K*R*T0/V;                    % decay constant [1/s]
C1   = 1;   % scaling factor
% --- Time vector ---
t = linspace(0,0.05,500);   % 0 to 0.05 s, 500 points
% --- Reservoir pressure vs time ---
P = P0*exp(-lambda*t);      % exponential decay [Pa]
% --- Exit velocity vs time (isentropic) ---
Ve = sqrt(2*gamma*R*T0/(gamma-1) .* (1 - (Pa./P).^((gamma-1)/gamma)));  % [m/s]
% --- Force vs time ---
F = C1 .* (K .* Ve + Ae * beta) .* P - Ae * Pa;  % [N]
% --- Moment of inertia ---
I = 0.5 * M * (r2^2 + r1^2);   % [kg m^2]
% --- Angular acceleration (Torque/I) ---
Torque = F * r2;              % [N·m]
alpha  = Torque ./ I;         % [rad/s^2]
% --- Angular velocity (integrate alpha over time) ---
omega = cumtrapz(t, alpha);     % [rad/s]
% --- RPM vs time ---
RPM = (omega * 60 / (2*pi));      % [RPM]
% --- Plotting ---
```

```
figure;
subplot(2,2,1)
plot(t,F,'b','LineWidth',1.5)
xlabel('Time [s]'); ylabel('Force [N]');
title('Force vs Time'); grid on
subplot(2,2,2)
plot(t,RPM,'r','LineWidth',1.5)
xlabel('Time [s]'); ylabel('RPM');
title('RPM vs Time'); grid on
subplot(2,2,3)
plot(t,P,'c','LineWidth',1.5)
xlabel('Time [s]'); ylabel('Pressure [Pa]');
title('Reservoir Pressure vs Time'); grid on
subplot(2,2,4)
plot(t,Ve,'g','LineWidth',1.5)
xlabel('Time [s]'); ylabel('Velocity [m/s]');
title('Exit Velocity vs Time'); grid on
sgtitle('CO_2 Cartridge Rocket Performance')
```

7.22 Active Rocket Fins Matlab

```
%%%%%%%%%%%%%%%%%%%%%%%%%%%%%%%%%%%%%%%%%%%%%%%%%%%%%%%%%%%%%%%%%%%%%%%%%%%%%%%%%%%%%%%%%%%%%%%%%%%%%%%%%%%%%
%%%%%%%%%%%%%%%%%%%%%%%%
clear; clc; close all;
%%
rho = 0.0023769;
d_in   = 6.6299;
spanD_in = 10.5433;
I_z = 0.05;
cg_in = 34.8852;  cp_in = 35.5550;
static_margin = 0.26;  L_in = 49.0790;
%%
delta = 5*pi/180;
Cl_alpha = 2*pi;
Ch_delta = 0.010;
delta_w = 100*2*pi/60;
delta_t = 0.5;
w = 0;  C_lp = -0.01;
%%
D_ft = d_in/12;
radius_ft = (d_in/2)/12;
fin_span_in = (spanD_in - d_in)/2;
fin_span_ft = fin_span_in/12;
```

```
c_avg_in = 1.31;
c_avg_ft = c_avg_in/12;
S_ft2 = fin_span_ft * c_avg_ft;
r_ft = radius_ft + 0.4*fin_span_ft;
%%
V = linspace(0,1300,200);
% RockSim max velocities (small fin)
V2_max_mph = 866.53;  V4_max_mph = 367.31;
mph2fts = 1.46667;
V2_max = V2_max_mph * mph2fts;
V4_max = V4_max_mph * mph2fts;
%% Roll & Hinge Moments
Nfins_list = [2, 4];
colors = {'b','r'};
Mroll = zeros(numel(V), numel(Nfins_list));
Mhing = zeros(numel(V), numel(Nfins_list));
Mnet  = I_z * (delta_w / delta_t);
for i = 1:numel(Nfins_list)
  N_fins = Nfins_list(i);
  for j = 1:numel(V)
     q = 0.5 * rho * V(j)^2;
     L_fin = q * S_ft2 * Cl_alpha * delta;
     Mroll(j,i) = N_fins * L_fin * r_ft;
     Mhing(j,i) = q * S_ft2 * c_avg_ft * Ch_delta * delta;
  end
end
%% PLOTTING
figure('Color','w','Position',[200 100 1100 400]);
subplot(1,2,1);
hold on;
plot(V, Mroll(:,1), 'b-', 'LineWidth', 2);
plot(V, Mroll(:,2), 'r--', 'LineWidth', 2);
xline(V2_max, 'b:', 'LineWidth', 1.2);
xline(V4_max, 'r:', 'LineWidth', 1.2);
text(V2_max+20, 0.85*max(Mroll(:)), sprintf('2 fins: %.0f ft/s', V2_max), 'Color','b');
text(V4_max+20, 0.65*max(Mroll(:)), sprintf('4 fins: %.0f ft/s', V4_max), 'Color','r');
xlabel('Velocity [ft/s]');
ylabel('Total Roll Moment [ft·lbf]');
title('Roll Moment vs Velocity');
legend('2 fins','4 fins','Location','northwest');
grid on; xlim([0 1400]); ylim([0, max(Mroll(:))*1.1]);
subplot(1,2,2);
hold on;
plot(V, Mhing(:,1), 'b-', 'LineWidth', 2);
plot(V, Mhing(:,2), 'r--', 'LineWidth', 2);
xline(V2_max, 'b:', 'LineWidth', 1.2);
xline(V4_max, 'r:', 'LineWidth', 1.2);
xlabel('Velocity [ft/s]');
```

```
ylabel('Hinge Moment per Fin [ft·lbf]');
title('Hinge Moment (Servo Torque) vs Velocity');
legend('2 fins','4 fins','Location','northwest');
grid on; xlim([0 1400]); ylim([0, max(Mhing(:))*1.1]);
sgtitle('Active Fin Roll Control — Small Fin Geometry, 2 vs 4 Fins');
fprintf('\n===== Geometry & Stability Info =====\n');
fprintf('CG = %.4f in, CP = %.4f in, Margin = %.2f, Length = %.2f in, Diameter = %.2f in\n',...
  cg_in, cp_in, static_margin, L_in, d_in);
fprintf('Fin span = %.2f in, mean chord = %.2f in, area = %.4f ft², r = %.2f in\n',...
  fin_span_in, c_avg_in, S_ft2, r_ft*12);
fprintf('\n===== Roll/Hinge Moments at RockSim Max Velocities =====\n');
for i = 1:numel(Nfins_list)
  N_fins = Nfins_list(i);
  V_rsim = (i==1)*V2_max + (i==2)*V4_max;
  q = 0.5 * rho * V_rsim^2;
  L_fin = q * S_ft2 * Cl_alpha * delta;
  M_roll_rsim = N_fins * L_fin * r_ft;
  M_hing_rsim = q * S_ft2 * c_avg_ft * Ch_delta * delta;
  M_servo_est = M_hing_rsim + Mnet/N_fins;
  fprintf('%d fins @ %.0f ft/s → Roll = %.2f ft·lbf | Hinge = %.3f ft·lbf | Servo ≈ %.3f ft·lbf\n',...
    N_fins, V_rsim, M_roll_rsim, M_hing_rsim, M_servo_est);
end
```